MIT Libraries | DSpace@MIT

MIT Open Access Articles

Additive Manufacturing of Functional Microarchitected Reactors for Energy, Environmental, and Biological Applications

Massachusetts Institute of Technology

Additive manufacturing of functional microarchitected reactors for energy, environmental, and biological applications

Seok Kim[1,2], Do Hyeog Kim[2], Wonpyo Kim[2], Young Tae Cho[2,*], and Nicholas X. Fang[1,*]

[1]Department of Mechanical Engineering, Massachusetts Institute of Technology, Cambridge, MA 02139, USA.
[2]Department of Mechanical Engineering, Changwon National University, Changwon, South Korea.
*Corresponding author: Young Tae Cho (ytcho@changwon.ac.kr) and Nicholas X. Fang (nicfang@mit.edu)

Abstract
The use of microreactors in the continuous fluidic system has been rapidly expanded over the past three decades. Developments in materials science and engineering have accelerated the advancement of the microreactor technology, enabling it to play a critical role in chemical, biological, and energy applications. The emerging paradigm of digital additive manufacturing broadens the range of the material flexibility, innovative structural design, and new functionality of the conventional microreactor system. The control of spatial arrangements with functional printable materials determines the mass transport and energy transfer within architected microreactors, which are significant for many emerging applications, including use in catalytic, biological, battery, or photochemical reactors. However, challenges such as lack of design based on multiphysics modeling and material validation are currently preventing the broader applications and impacts of functional microreactors conjugated with digital manufacturing beyond the laboratory scale. This review covers a state-of-the-art of research in the development of some of the most advanced digital manufactured functional microreactors. We then the outline major challenges in the field and provide our perspectives on future research and development directions.

Keywords
Microreactor, Architected materials, Additive manufacturing, Micro-/Nano-fabrication, Functional materials

1. Introduction
Microreactors are widely used in modern chemical process engineering because of their energy efficiency, scalability, safety, and finer degree of control. Unlike large traditional batch reactors, microreactors are constructed from a network of miniaturized reaction structures in configurations measured in millimeters and embedded with micrometer-sized pores or channels. Devices with these small dimensions provide a more efficient mass and heat transfer because of their large specific surface areas, resulting in a higher yield of reaction performance (Fig. 1A-B) [1]. With the development of microfluidic systems, these microreactors have enabled the effective manipulation and control of working fluids that are geometrically constrained within environments having internal dimensions, or hydrodynamic diameters. As a result, advances in a microreactor have gained increasing importance in chemical, pharmaceutical, and energy applications in the recent decades. Furthermore, the economic advantages and improved safety metrics of microreactors for production purposes have further encouraged their adoption in real industrial applications. A number of manufacturing technologies for microreactors, including hot embossing, laser ablation, micromachining, and chemical etching, are currently commercially used. These techniques are generally constrained in design to two-dimensional (2D) planar channel networks, with more intricate designs leading to significant increases in cost, manufacturing complexity and production time. Thus, they do not allow for the design complexity, such as the incorporation of intricate three-dimensional (3D) mixing pathways. The

viscosity has a dominant effect in the microscale because of the shear force, which is inversely proportional to the thickness of fluid film in motion, hence achieving a nearly perfect mixing in a shallow well or channels in the 2D geometry is difficult. This mixing issue can be easily solved if the well or channel incorporates 3D structures. Here the use of additive manufacturing (AM) is a promising solution for fabricating microreactors to allow the incorporation of innovative designs, which have previously been limited to simple planar microfluidic devices [2]. Indeed, the concept of 3D microreactors by AM technology has a long history and Ikuta et al. introduced a microscale AM technique that can be utilized for microfluidic systems and biochemical microreactors [3-6]. They suggested the concept and vision of 3D microfluidic systems integrated with a silicon process for the electronic components and a polymeric AM process for the fluidic components [3-6]. Far ahead of their time, they also proposed the big picture in this field, including the biochemical microreactor-on-an-integrated circuit (IC) chip system, multiscale integrated microreactors, multifunctional microreactors, and the need for mass production of a 3D microreactor system (Fig. 1C) [6]. To meet a large demand for an analytic understanding of the biological system, the authors suggested the basic design of a 3D micro-chemomechatronics device based on a real biological cellular system. To date, 3D microreactors technology remains a high-barrier-of-entry technological field because the manufacturing, materials, and integration processing have not yet matured enough to implement those concept and visions [2, 7]. These challenges initiated an opportunity for the 3D microreactors to explore advanced 3D microfabrication technologies that are at various stages of research and development.
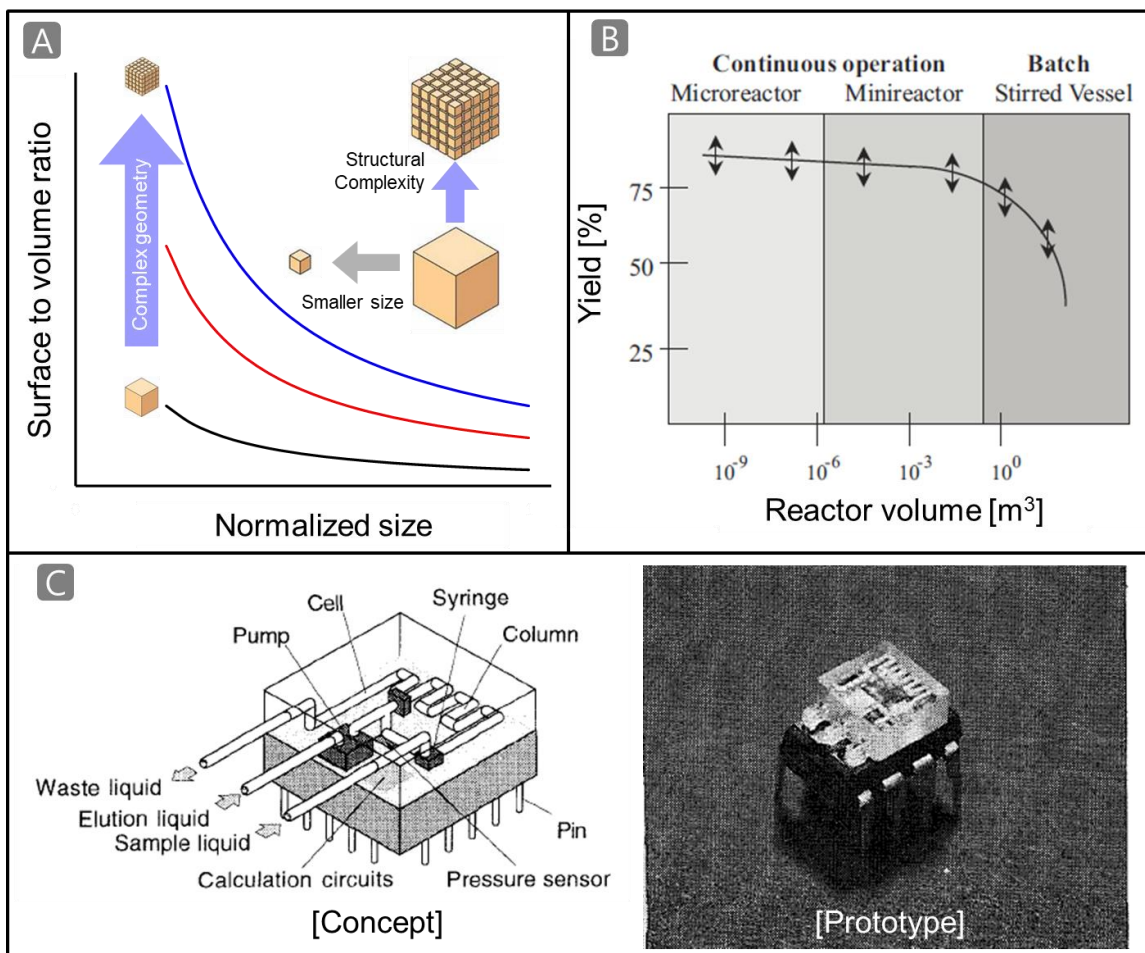
Figure 1. A microreactor can lead to increased yields through high surface-to-volume ratio and rapid mixing. (A) The surface-to-volume ratio exponentially decreases with the cell size, while the total volume remains constant; small cells have a high ratio; and large cells a low ratio. (B) General plot of the yield, as a measure of the reactor performance, versus the reactor volume. Only a slight decrease is found when increasing the reactor volume from 10^{-9} to 10^{-3} m^3, and this is referred to as the micro- and mini-range. A further increase in volume, also accompanied by a change from continuous to batch processing, results in a considerable performance decrease. Reprinted from reference [1] with permission. (C) Conceptual schematic and prototype of a 3D microfluidic reactor with an IC chip for a biochemical analyzer, before two decades ago Reprinted from reference [3-6] with permission.

We have recently entered a new era of AM (or 3D printing) that is a key enabler to the fabrication of complex, multiscale architectures and leads to previously unobtainable combinations of structural, mechanical, chemical, thermal, and functional properties [8-9]. AM is particularly attractive in the microreactor technology field because its fabrication method allows precise control over the topology, geometry and composition of the designed functional reactors [10]. AM also provides a mass customization, multimaterial fabrication, and the ability to produce parts with a complex geometry. For small production runs, AM may be economical, and allows for an environmentally friendly efficiency (minimum waste and tooling). More importantly, AM benefits from the compatibility of the digital design interacting with CAD tools that can design additive manufactured devices in modules and predict the performance with finite element tools prior to fabrication.

AM is transforming the microreactor paradigm to functional microarchitected reactors by combining AM methods with advanced materials used for AM and digital freeform design. Architecture has always played an important role in material properties and the mechanical efficiency of structures [4]. Materials with architected microstructures can achieve a higher structural efficiency. Furthermore, architecture provides an additional degree of freedom in the material design. Architected materials (i.e., adding architectures into materials) offer the opportunity to tailor the physical properties. The device performance is also fundamentally controlled by geometry at multiple length-scales. The combination of geometry with material properties determines the behavior of architected materials, which are significant for many emerging applications, including in catalytic, biological, and battery reactors and other photochemical reactors. Therefore, considering the architected materials and the digital design used for AM with the microreactor technology, the term "microreactors" is no longer valid, and should be replaced by the term "microarchitected reactors (MAR)", which can cover all aspects of 3D structural design and materials of emerging microreactor technologies (Fig. 2). This transition is dependent on the advances in the technologies and materials for AM as well as on improved digital design methods.

This review covers the recent advancements in AM that are making the paradigm of functional MAR a reality. We first describe the tools for AM, including established and emerging methods, materials used in AM, and design/modeling that enable the production of functional MAR devices. We then discuss different AM applications for the chemical/catalytic MAR, bio/pharmaceutical MAR, and energy MAR. Many of the application areas are emergent, and many challenges still exist to realize the full vision of additively manufactured functional MAR. We conclude with an outlook on the future challenges and opportunities in this exciting area.
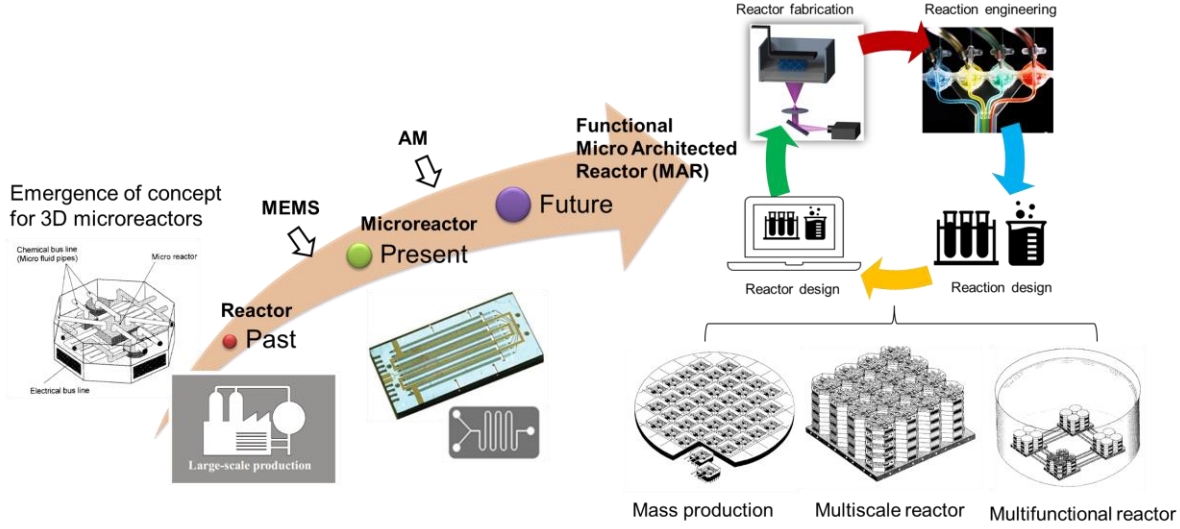
Figure. 2 Our perspective for the future microreactor technology along with AM technologies, digital design, and functional material. Example of the iterative process of design, fabrication, and reaction for the functional MAR. Note that some pictures have been reproduced from ref. [3-6] with permission.

2. Tools for AM of functional microreactors

This chapter provides a brief overview of the key components for AM that will enable the functional MAR with an emphasis on the AM technologies and materials and digital design.

2.1 Established AM methods

Variations on AM methods have recently focused on improving spatial resolution, printing speed, and production quality on integrating multiple materials in of printed 3D constructs. These advances have transformed AM from a technique for rapid prototyping to an established technology that is transforming industrial production. However, most AM technologies are limited to a narrow range of materials, and the fabrication of functional devices is still greatly hindered by limitations in size, resolution, or complexity. The resolution-to-manufacturing time ratio (RTM, expressed with units of 10^{-3} m^2 min^{-1}) was developed as a quantitative metric to compare the efficiency of different AM techniques and further classify various AM technologies in terms of fabrication efficiency (Fig. 3, Equation (1)) [11].

$$\text{RTM} = \frac{\text{Spatial resolution}}{\text{Time for manufacturing}} \cong R \cdot P = \frac{1}{d} \cdot \frac{V}{t} \tag{1}$$

R is the best spatial resolution achieved within the printing technology, expressed as the inverse of the minimum feature dimension (d, measured in m). P is the delivery rate of the material being printed or assembled, which is a function of the volume (V, measured in m^3) delivered per unit of time, t (in minutes). Note that R or P may vary depending on the materials delivered, the geometry, and the printing parameters. Figure 3 represents the distribution of the various AM technologies in the parameter space with axes of the d and P axes. The contour lines of the RTM ratio are plotted. The higher the value of the RTM ratio, the more efficient the process. Most AM technologies are placed along the diagonal of the "*d-P*" parameter space, indicating that constructing fine details results in lower delivery rates, which are represented by ovals in the figure.
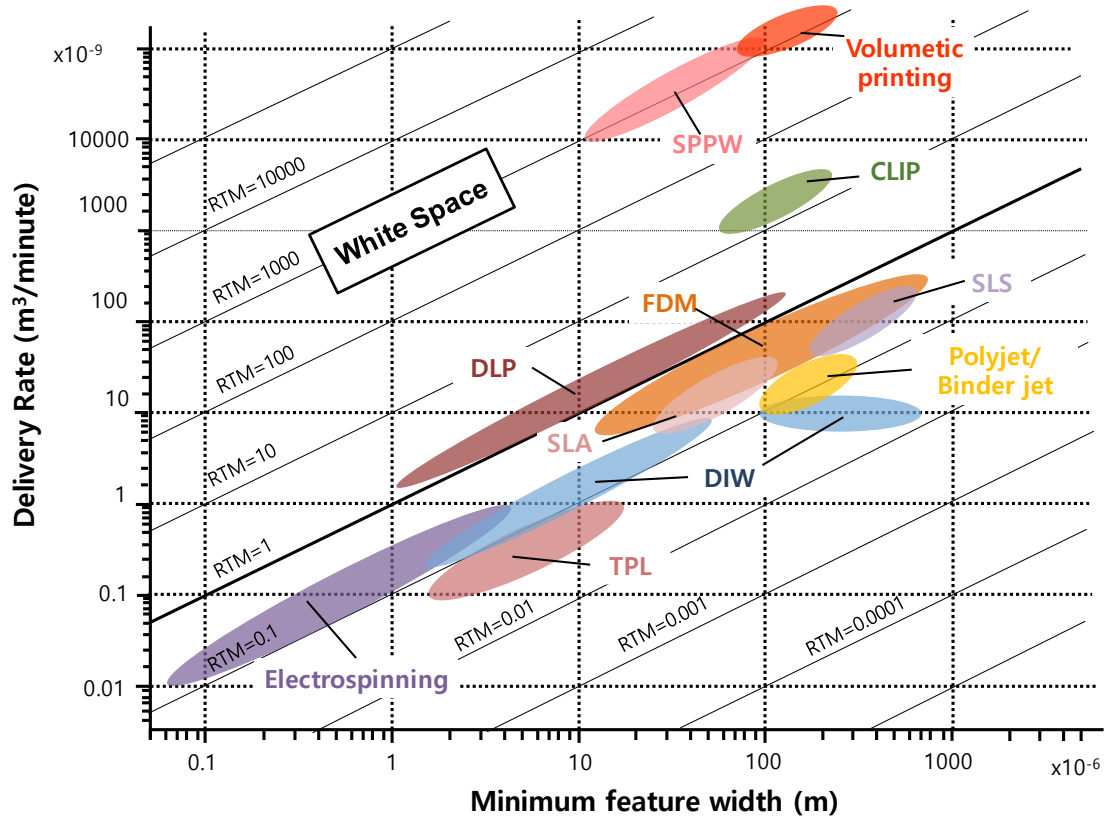
Figure 3. The solid lines represent the resolution/time for manufacturing (RTM) ratio [10^{-3} m^2 min^{-1}] of figure that ranks various AM technologies according to their efficiency, considering the minimum feature width (*x*-axis) and fabrication throughput (*y*-axis). A larger RTM ratio represents a more efficient printing process. The reported values are an estimate of the possible values achievable with the technology. The true RTM ratio can differ from the value in this figure based on the printing parameters, materials used, and required resolution. Reprinted from reference [11] with permission.

2.1.1 Printing with light

AM technologies with light operate by solidifying the components in specific voxels of a photosensitive material in response to an introduced UV light or laser source to form the desired 3D objects (Figure 4). Selective laser sintering (SLS) is based on a beam of light focused at defined regions of a powder bed, which utilizes a laser source to sinter or fuse polymeric powders in a heated powder bed by a raster-like pattern layer upon layer. After each 2D layer, a new layer of powder is spread across the powder bed by a roller for resupply before sintering another layer on top of the previously fused one. Once the 3D construct has been fabricated, it is removed from the bed, and might undergo further heat treatment in a furnace. SLS is commonly used in the production of a variety of thermoplastic polymers, metals, ceramics, mixtures of polymer-ceramic, and polymer-encapsulated ceramic. However, the poor flowability caused by the high interparticle frictional forces in SLS limits the high quality and consistency of a 3D printed structure. The estimated RTM ratio for SLS is ~ 1×10^{-3} m^2 min^{-1} [12-13].

Stereolithography (SLA) is the first AM method made available. It typically uses a UV light to cure a photosensitive resin layer upon layer by pointwise photopolymerization, which offers a high resolution of approximately 25 µm and few constraints on geometry. SLA applies a similar mechanism as SLS. Liquid resin is cured into a solid form in the regions of light exposure upon irradiation. The process continues by

adding new liquid resin to the reservoir and generating the 3D constructs layer by layer. The estimated RTM ratio is ~ 0.5×10^{-3} m^2 min^{-1} [14-16].

Meanwhile, two-photon lithography (TPL), which is also known as direct laser writing, involves the use of a non-linear multiphoton polymerization process, which provides a high spatial resolution of the final object down to a sub-micron scale with voxel-by-voxel printing (a voxel is defined by a physical object of a collection of finite volume elements). Although the spatial resolution of this AM process has improved, further progress in both material development and fabrication rate is needed. The RTM ratio is ~ 0.05×10^{-3} m^2 min^{-1}, indicating that TPL has a very high resolution despite taking a long time to manufacture large structures [15-17].

Recent advances in photolithography-based AM have introduced new methods to increase production speed. Digital light patterning (DLP) exploits a digital micromirror device (DMD) or liquid-crystal display to project a 2D pattern into the reservoir, enabling the solidification of an entire layer in a single exposure. Subsequently, the platform is vertically translated, and the process is repeated layer by layer until the complete fabrication of the 3D object. The polymerization thickness lies between 10 µm and 100 µm, which is dependent on the penetration depth of the light source caused by the combined effect of the photosensitive resin characteristic and several key process parameters, including light source power, exposure time, and photoinitiator concentration [15-16]. Although the primary material for the DLP process is based on polymers, other types of materials, such as ceramics, could also be printed by a pre-ceramic polymer resin. Furthermore, a multimaterial approach, which could be used for multifunctional devices or shape-shifting architectures known as four-dimensional (4D) printing [18], has been reported. The estimated RTM ratio of the DLP is up to 2×10^{-3} m^2 min^{-1} [15-16, 19-20].

Continuous liquid interface production (CLIP) is an upgraded variant of DLP printing, which significantly increases the production rate of light-based AM by introducing an oxygen permeable window below the liquid resin bath. The oxygen rich zone, which inhibits photopolymerization at the interface between the window and the growing part, can continuously print parts, thereby removing the need for a sequential layer-by-layer process. The estimated RTM ratio is significantly increased to ~ $5\text{-}10 \times 10^{-3}$ m^2 min^{-1}, and remains one of the most efficient AM technologies [21].

The self-propagating photopolymer waveguide (SPPW) takes advantage of the non-linear optical effect that traps the UV light in a waveguide if the index of refraction changes on polymerization. The SPPW could be used to fabricate lattice-type structures with the maximum available thickness of several centimeters and the minimum strut diameter of the lattice unit cell of about 10 µm [15, 22]. The lattice structure is fabricated by a single 2D exposure plane instead of a stacked layer-by-layer approach. If a mask with a 2D pattern of apertures is simultaneously exposed to multiple collimated beams originating from different directions, an array of waveguides will form from each of the collimated beams. The waveguides will polymerize together at the points of intersection, or nodes, creating a self-supporting, open-cellular lattice structure. The SPPW method is 100-1000 times faster than the traditional layer-by-layer methods with one short exposure (1-2 min), which enables the fabrication of 3D structures at a higher rate with an estimated RTM ratio of ~1 m^2 min^{-1} [15, 22]. However, only features linearly extending from the exposure surface can be grown; hence, the ability is limited to the fabrication of lattice-type structures.

2.1.2 Printing with material deposition

Although light-based AM methods provide high resolution (Fig. 3), they are limited to printing with photosensitive materials. In contrast, deposition-based AM methods are capable of utilizing myriad materials in the form of printable inks that are formulated from a wide range of molecular, polymeric or

particulate species [15, 23-27]. Deposition-based AM functions by depositing material in specific voxels to fabricate the desired 3D object (Fig. 4).

Fused deposition modeling (FDM) has been extensively used to print the desired structures via molten thermoplastic polymers extruded into filaments. The melted filament is deposited layer-by-layer until the 3D structure is completed. The melted filament rapidly cools down below its glass transition temperature and solidifies again upon contact with the ambient air. FDM is mainly used for thermoplastics, but the filaments could be filled with other composite materials, such as carbon black, carbon fiber, wood, metallic powders, and ceramic powders, to enhance the functionality or mechanical properties of the printed part. FDM has an estimated RTM ratio of ~ 1×10^{-3} m^2 min^{-1} [15, 23].

Unlike in the FDM method, direct ink writing (DIW) extrudes a viscoelastic or viscoplastic ink in a syringe through a nozzle onto the printing bed under an external force, such as piston-, pneumatic-, or screw-driven robotic dispensing, thermal or piezoelectric actuators, and laser-induced forward transfer. DIW is typically done under ambient conditions, although the ink and bed could be heated or cooled to a desired temperature using a heating or cooling compartment. The DIW process can use a wide range of materials, including ceramic and carbon materials, aerogels, and biomaterials, which is favorable for catalytic materials. However, one of the main limitations of DIW is the low mechanical properties of the viscoelastic ink that prevent the robust formation of resulting structures. Therefore, post-processing techniques such as sintering or curing is typically required to improve the structural integrity. The RTM ratio achieved with DIW is in the range of ~ 0.1-0.5 $\times 10^{-3}$ m^2 min^{-1} [15].

In addition to FDM and DIW, several types of direct jetting-based AM methods can also be used (i.e., polyjet printing and binder jetting). Polyjet printing is a combination of both deposition-based and light-based AM methods, in which it uses a photosensitive polymer droplet that polymerizes upon exposure of the UV source. Binder jetting operates by ejecting a droplet of a binder solution onto a powder bed, forming adhered particles in the region where the binder is printed. The solvent binds the powder, forming a slice of solid material. Subsequently, a new layer of powder is laid down, and the process is repeated to build the 3D structures in a layer-by-layer fashion. The estimated RTM ratio of this approach is ~0.1×10^{-3} m^2 min^{-1}, with a medium level of manufacturing efficiency [24-25].

Electrospinning is a common technique used to produce interwoven meshes of thin polymeric fibers. Electrospinning involves an electrohydrodynamic process, during which a liquid droplet is electrified to generate a jet, followed by stretching and elongation to generate fibers. A high-voltage electric field is applied to create an electrically charged jet of a polymer, which is ejected from the tip of a Taylor cone and gathered on a grounded collector. Despite being a relatively old technology, electrospinning is a versatile and viable technique for generating ultrathin fibers. Remarkable progress has been made with regard to the development of electrospinning methods to enable various applications such as catalytic supports, energy/environmental components, and photonic/electronic devices, and biomedical scaffolds. Electrospinning has an RTM ratio of approximately 0.1×10^{-3} m^2 min^{-1} [15, 26-27].

2.1.3 Emerging technologies in AM

The promising advances that aim to tackle the throughput-associated concerns regarding AM techniques are exhibited by the volumetric AM technique beyond the conventional layer-by-layer process. These emerging light-based volumetric AM approaches are based on the use of multiple projection image superposition via holographic, computed tomographic reconstruction, or combining multiwavelength source in parallel [28-30]. The holographic volumetric AM could fabricate complex millimeter-scale 3D polymeric geometries in the span of a few seconds without any supporting structures. This approach is implemented via the superposition of holographically patterned light fields from multiple beams to be cured

3D objects. Tomographic volumetric AM has recently been introduced as a method for rendering a solid, 3D object within a rotating photopolymer resin bath. Computed axial tomography is used to project an evolving light pattern into the rotating bath to build complex 3D shapes during a single exposure. In another emergent approach, the volumetric AM through dual wavelength is employed for two perpendicular irradiation patterns at the blue and near-UV wavelengths to independently control either polymerization initiation or inhibition, respectively, for the volumetric photopolymerization in bulk resin. The RTM ratio of these volumetric AM technologies is ~ 1 m^2 min^{-1}. While these volumetric methods are not yet mature and applied for microreactor fabrication, they could comprise another technology that avoids conventional layer-by-layer processing and enables a concurrent solidification of all voxels that comprise a 3D object.
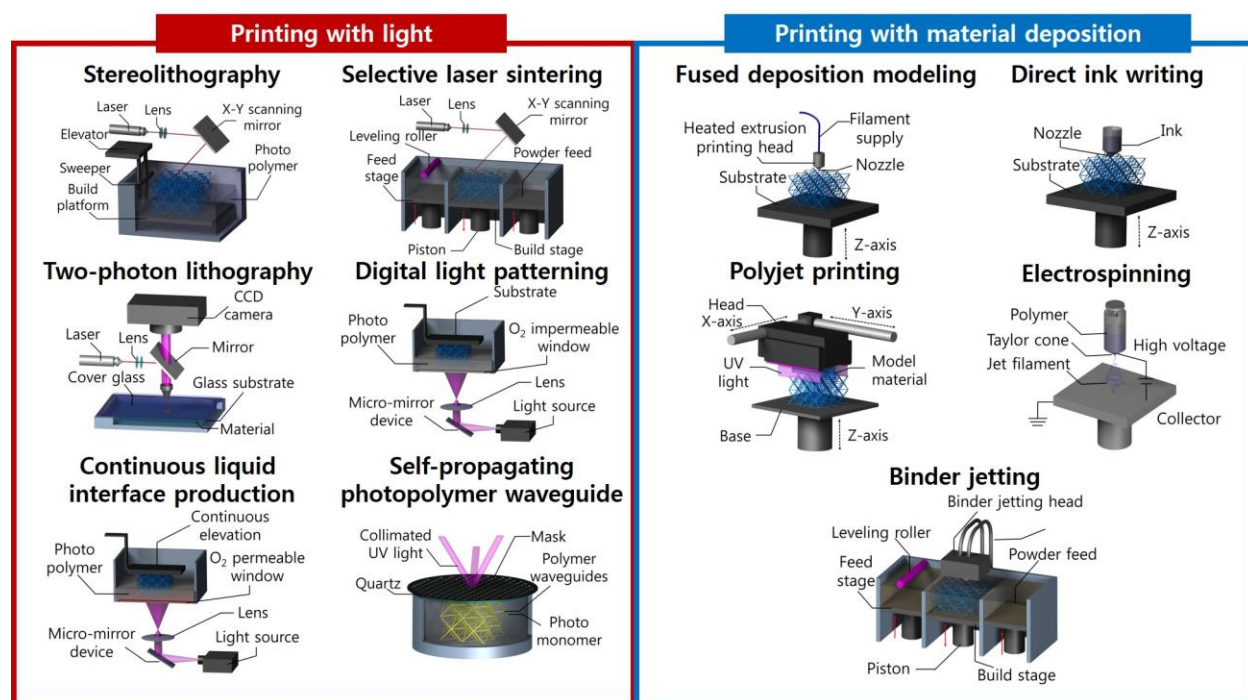

Figure 4. Commonly used AM technologies in functional microreactors. Left: light-based technologies (stereolithography [14-16], selective laser sintering [12-13], two-photon lithography [15-17], digital light pattering [15-16, 19-20], continuous liquid interface production [21], and self-propagating photopolymer waveguide [15, 22]). Right: deposition-based technologies (fused deposition modeling [15, 23], direct ink writing [15], polyjet printing [24-25], electrospinning [15, 26-27], and binder jetting [24-25]).

2.1.4 Current fabrication technology limitations

Both AM methods have some limitations and challenges to address prior to being applied in the functional MAR technologies. Despite the system improvements in the AM technologies, the overall part size (and fabrication speed) is traded off against the resolution and minimum feature size, as shown in RTM analysis (Fig. 3). The small feature size is incompatible with a large-throughput fabrication; therefore, the existing AM technologies tend to cluster by following the universal trend (representing the scaling law) (*d-P* plot, Fig. 3). Behind this scaling law lies the discretized voxel (i.e., controlled volume elements acting as informational units similar to digital bits) throughput within the AM methods. Reducing the voxel dimensions will significantly slow down the AM process. In 2PP, for example, reducing the voxel size by 10 times will simply result in the 10^3 times increase of the fabrication time because of its point-by-point scanning mechanism. Thus, the scaling problem of increasing the voxel throughput without compromising

8

the resolution remains a challenge in AM technologies. We expect future AM methods to overcome this scaling limit for the emerging MAR applications. Furthermore, based on the given functional requirements, the design framework begins with the selection of AM processes and the related material options. Although the AM methods have shown great advantages in fabricating multifunctional structures, there are still several problems that need to be addressed. The kinds of materials that are available for the multimaterial AM methods are usually limited [10, 31-32]. Broadening of the material library that can be additive manufactured and enabling novel composites are critical tasks in the future.

AM-printed parts often show poor surface quality when compared to the smooth surfaces of parts produced by subtractive manufacturing [33]. This stems from the available voxel size and layered nature of AM technologies, resulting in an inherent surface roughness inside the microchannels of the reactors and lowering the transparency of the printed reactors. Direct optical access would be a major advantage when monitoring of the chemical reaction in the channel interior is desired [34]. The surface roughness could also have an unexpected effect on the fluidic characteristics of the microreactor devices, such as mixing points, flow paths, and residence volumes [35]. Thus, the improvement of the AM methods of the functional MAR is needed to control the surface roughness of the reactor internals.

2.2 Design and modeling

AM technologies provide a rapid interaction between a computer model of 3D objects and their fabrication, creating an the opportunity for computational topology optimization of the desired 3D structures [36]. This section briefly discusses modeling and design tools to characterize the transport phenomena in flowing systems and reactor engineering. First, the computational fluid dynamics (CFD) is introduced to characterize hydrodynamics and heat and mass transfer in fluidic system reactors. Second, the topology optimization method is described to fully leverage the AM capabilities combined with the materials used according to the target application.

2.2.1 Computational fluid dynamics

The flow distribution in microreactors has been intensively studied in order to properly optimize the overall performance of the functional architected reactors. CFD provides the numerical solution of conservation equations for mass, momentum, and energy in a flow geometry of interest and the design optimization by modeling the hydrodynamics of the flow reactors. The governing equations are not scale-dependent, and can, therefore, be applied to a wide range of problems and length scales, from microreactors to large-scale systems. The analysis of the hydrodynamics inside microreactors is directly utilized to control the different variables, including channel shape and size, internal walls, mixer structure, and fluidic conditions (e.g., flow velocities and temperature). As shown in Fig. 5, this knowledge captured from CFD can be coupled with experimental studies for a further design analysis. Several commercial software packages that are either based on the finite element method (FEM) (e.g., COMSOL) or the finite volume method (FVM) (e.g., Ansys Fluent) are available. These computational tools can use a database of properties for the available materials and inform on the proper print parameters and material choices to design the final part. The geometry in the FEM is discretized by finite elements interconnected at nodal points, while that in the FVM is subdivided into finite volumes enclosing the nodal points of the mesh. As a result, the FVM is a more robust method for computing hydrodynamics and associated transport phenomena. In contrast, the FEM is better suited for solving coupled multiphysics problems involving several domains (e.g., the coupling between the chemical reaction rate and the fluidic transport in a given structure). For example, a solution is pumped through a catalytic reactor where a solute species reacts as it gets in contact with the catalyst. The CFD analysis can find an optimal catalyst distribution to maximize the total reaction rate for a given total

pressure difference across the reactor. The catalyst distribution of the catalyst determines the total reaction rate in the reactor. A large amount of catalyst results in a low flow rate through the reactor. In contrast, less catalyst gives a high flow rate, but low conversion of the reactant. The CFD is also capable of performing shape-based optimization. Starting from a pre-defined starting geometry and the corresponding CFD results, the parametric change analysis to this geometry enables the optimization of a target function (e.g., for pressure drop minimization). Although the resultant optimized "digital geometry" is difficult to fabricate via traditional machining methods, AM can bridge this gap between digital geometry from the CFD and the substantial physical object.
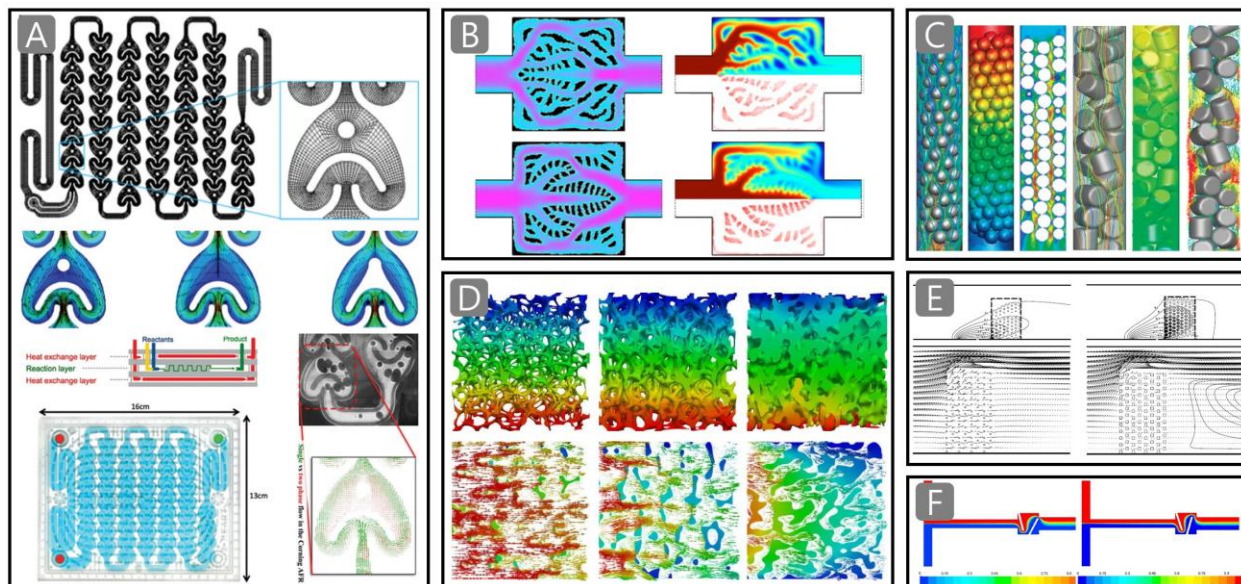

Figure 5. Examples of the CFD application in microreactor geometries. (A) Numerical study of flow hydrodynamics at different flow rates in three different reactors. Reprinted from reference [8] with permission. (B) Optimization of the structured catalytic microfluidic reactors. Reprinted from reference [37] with permission. (C) Simulation results of the flow field and pressure drop in a fixed-bed reactor. Reprinted from reference [38] with permission. (D) Characterization of the temperature field and velocity vectors inside porous substrates [39], (E) Simulated temperature contour in fixed-bed microreactors. Reprinted from reference [40] with permission. (F) Optimization of a mixing unit for a chemical microreactor. Reprinted from reference [41] with permission.

2.2.2 Topology optimization

Computational topology optimization offers a systematic framework for an efficiently architected material design to control mechanical, thermal, and fluidic properties. Topology optimization has been developed to define the ideal arrangement of two or more materials to achieve optimum macroscopic properties. For example, powerful computational tools, such as commercial software Altair OptiStruct [42] and Autodesk Within [43], were recently developed to optimize structures for mechanical efficacy. Accordingly, a structurally efficient and lightweight architecture for a complex-shaped part can be computationally determined with this topology optimization methods. A typical optimization starts with a solid part and removes the material, whereby the user can choose to either achieve a favorable volume reduction or meet defined load requirements. A typical example of the topology optimization design framework is as follows [36]. For a given target application requiring multiple functionalities, the designer may develop a porous microarchitected material to satisfy minimum mass, isotropic stiffness, and minimum fluid permeability. Given these inputs and relevant manufacturing parameters, the topology optimization algorithm returns an

optimized unit cell architecture that satisfies all the design requirements. As shown in the example illustrated in Fig. 6A, the optimized unit cell architecture is then repeated in all directions and manufactured to form the bulk material. The improving fluidic properties have drawn interest from the topology optimization due to the necessity of fluid flow in a number of applications, from biomedical scaffolds to thermal transport and catalytic reactors (Fig. 6B-C). With the topology optimization methods, the reactor structure is initially not known but gradually forms through an iterative process, guided by the problem optimization. The great advantage of topology optimization is that the complexity of the final solution is unconstrained and, therefore, not burdened by our preconceived expectations. This method has recently been successfully applied in designing optimal catalytic microreactors [44] and bioreactors [45].
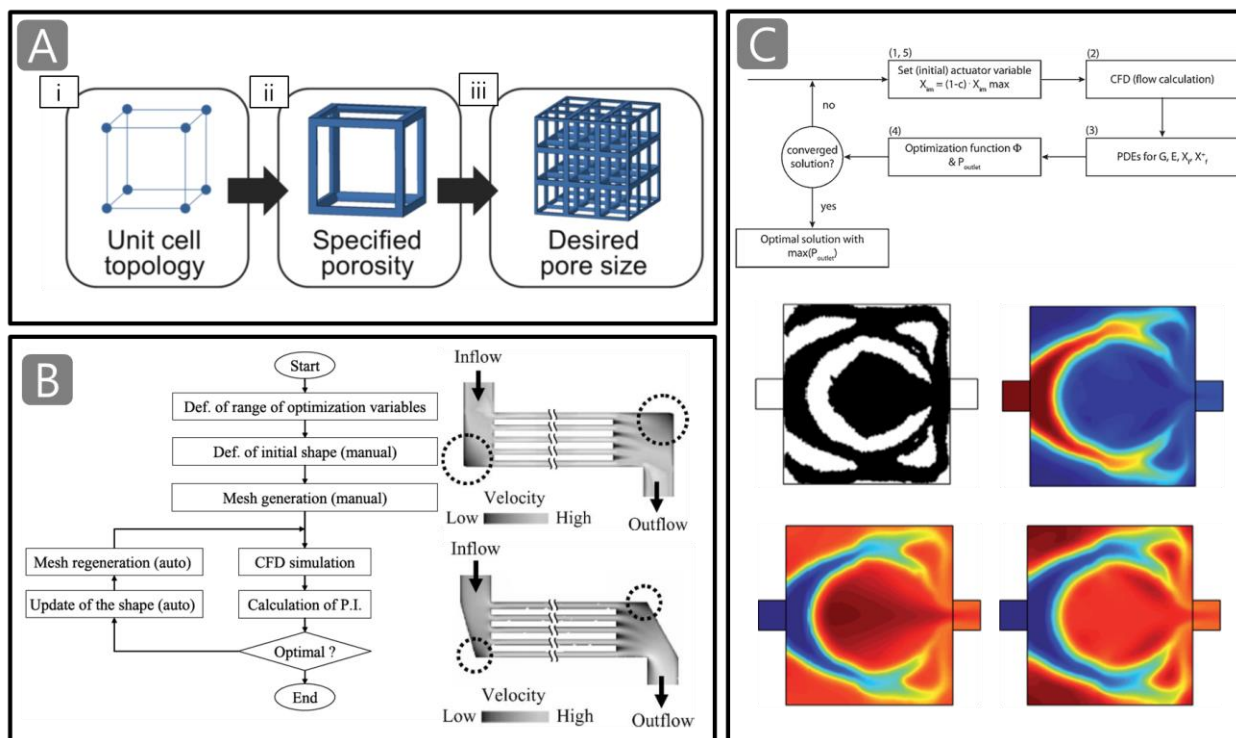

Figure 6. (A) 3D microlattice design approach for tissue engineering. (i) A defined topology is used to construct unit cells with (ii) a specified porosity for (iii) generating a lattice structure with desired pore sizes. Reprinted from reference [46] with permission. (B) Optimization for the design of plate-fin microdevices. Reprinted from reference [44] with permission. (C) Microbioreactor with the topology optimization process. Reprinted from reference [45] with permission.

2.2.3 Current modeling limitations

Although the CFD can analyze the fluidic transport, heat/mass transfer, and the kinetic modeling of microreactors where the reaction occurs in the bulk of the fluid, the detailed surface and fluid-phase chemical reactions occur on the reactor surface. Thus, a multiscale modeling approach is required to capture the different length- and time scales of species transport in the bulk fluid, adsorption on a surface, and subsequent chemical transformation [10]. The structural difference of models across scales is a critical challenge in multiscale modeling. The CFD treats the fluid flow as a continuum and captures only the bulk movement. We need to consider the chemo-physical processes on the reactor surface in a discrete manner to resolve individual molecules and capture stochastic events with certain probabilities. In addressing this issue, most of the developed models use one-way coupling by passing the parameters extracted from the

11

molecular-scale model to the continuum scale. For the molecular-scale modeling, the molecular dynamics or kinetic Monte Carlo can be used to represent the chemo-physical properties; however, note that they are restricted to limited time and length scales because of excessive computational resources. Therefore, the common approach is to couple the macroscopic approach of the CFD for continuum modeling and the molecular-scale simulations for parameter extraction. Most design methods are based on an iterative process of computer-aided simulation work (e.g., CFD) to optimize the design parameters. However, the CFD is computationally expensive, and relies on an accurate input of structural loads and material properties. Consequently, the computational load reduction is an emerging topic, especially when the capability of AM extends to multiple materials with complex shape and topology.

3. Applications of additive manufactured functional microreactors

The advances in AM technologies and digital design tools have enabled the realization of several functional microreactors. We introduce herein three emerging applications of additive manufactured microreactors that focus on the areas of chemical/catalytic, biological/pharmaceutical, and energy/environmental applications.

3.1 Fluidic microarchitected reactors

Although microfluidics is now a mature field, AM enables the fabrication of geometrically optimized microfluidic reactors. The shape and design of conventional fluidic reactors are limited by their manufacturing cost and the limitations of conventional manufacturing technologies. In the last few years, AM has been increasingly employed to fabricate microfluidic chips to reduce the time needed to transition from a concept to a chip device and add functional elements into the microfluidic chip that enable the on-chip mixing of fluids and the generation of fluid gradients. Directly additive manufactured microreactors with dimensions that match the required economical throughput is not yet feasible; however, AM methods could be used to improve the performance of conventional reactor layouts through optimized internal structures.
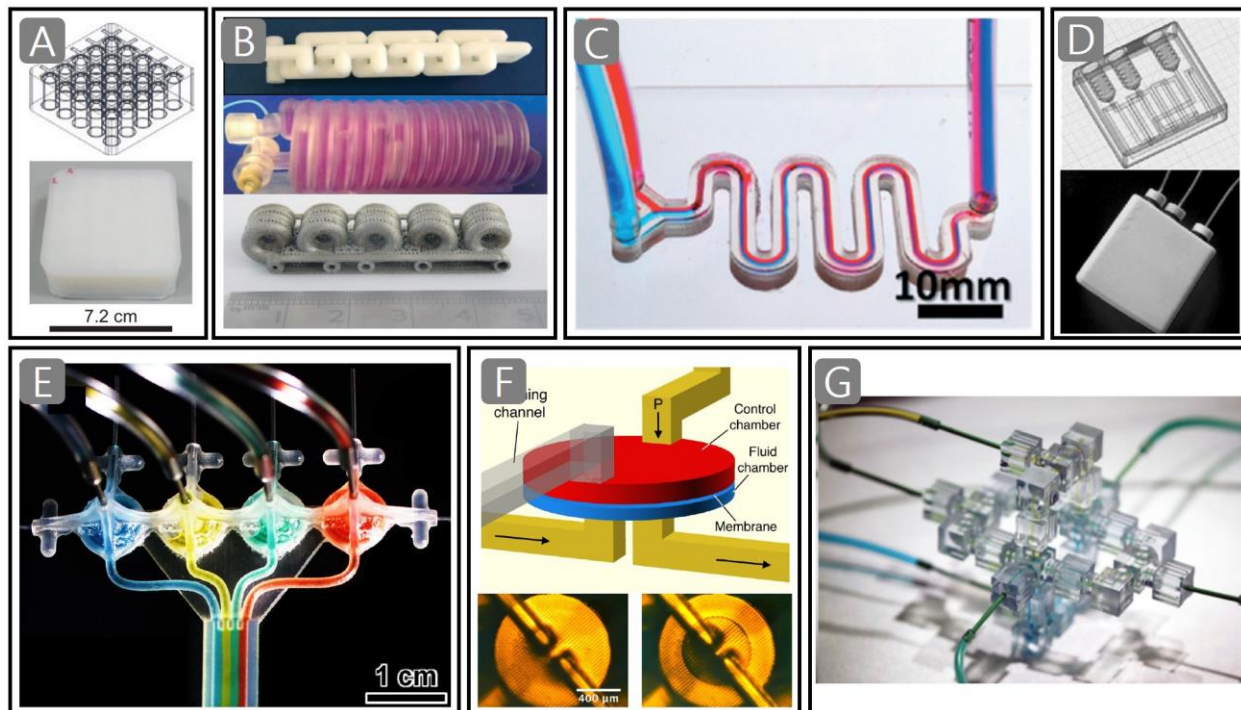
Figure 7. (A) 3D reactionware for the high-throughput solvothermal synthesis of a metal–organic framework. Reprinted from reference [47] with permission. (B) 3D-printed micromixers. Reprinted from reference [48] with permission. (C) Transparent microfluidic mixer. Reprinted from reference [34] with permission. (D) Microfluidic reactors for a catalytic synthesis. Reprinted from reference [49] with permission. (E) 3D pressure-actuated multiflow controller. Reprinted from reference [50] with permission. (F) 3D-printed membrane valve. Reprinted from reference [51] with permission. (G) Modular microfluidics. Reprinted from reference [52] with permission.

The internal structure needs to realize the desired mixing regime when combining multiple reactants or phases in a flow microreactor. Cronin and et al. demonstrated that the building of polymeric materials enables the direct use of custom 3D-printed reactors, called "reactionware" for chemical synthesis and analysis [53]. They also demonstrated how reaction vessels could be printed via DIW and how to insert non-printable components during pre-programed pauses in the printing chamber. Interestingly, this approach not only enabled chemical reactions to be monitored in-situ, but also allowed a reversal of selectivity for the obtained product. Another example of a customized reactor used for a synthetic workflow is the high-throughput reactor fabricated by FDM (Fig. 7A) [47]. In this context, the 3D-printed array reactor was developed to increase the range and versatility of reactor devices for use in a hydrothermal synthesis. Capel et al. introduced common AM techniques in the flow chemistry and compared each process. They raised the issue of the low optical transparency caused by the internal surface roughness resulting from the common AM materials, such as polymer and metals (Fig. 7B) [48]. To avoid this issue, Folch et al. demonstrated the fully transparent bio-microfluidic devices between two glass surfaces printed by DLP printing (Fig. 7C) [34]. In a different example, Benaglia et al. tested for a catalytic stereoselective Henry reaction via FDM-printed flow reactors. Subsequently, AM flow reactors were designed and fabricated from different materials to enable the catalytic synthesis of biologically active targets through a two-step continuous-flow process inside the customized reactors (Fig. 7D) [49].

Apart from the optimization of passive elements in flow reactors, AM allows for a direct integration of dynamic physical elements to manipulate the flow before, after, or inside the fluidic reactors. Lin et al. utilized the multimaterial ink-jetting (i.e., polyjet printing) process to manufacture active microfluidic

operators with complex geometries, including fluidic capacitors, fluidic diodes, and fluidic transistors (Fig. 7E) [50]. They evaluated the possibility of an on-chip automation of integrated fluidic systems and investigated the theoretical and experimental approaches to tuning the control parameters of each functional component. Meanwhile, Nordin et al. demonstrated DLP-printed microfluidic devices with active operators, such as valves and pumps (Fig. 7F) [51]. The device with a sandwiched valve of a 20 µm-thick membrane enabled a dynamic mixer of working fluids with serial multiplexing and the combination of multiple valves. The modular design is an inherent part of the AM technologies. SLA-printed polymeric discrete elements for 3D microfluidics with packaged connectors can be built as interlocking modules, and are easy to operate (Fig. 7G) [52]. Malmstadt et al. developed a sample library of standardized components and connectors to build large-scale microfluidic systems in 3D, which are modular and reconfigurable. This assembly strategy allows for a predictable fluidic system design by simple network analysis techniques (e.g., classical electronic circuit design).

3.2 Biological microarchitected reactors

The microfluidic reactor serves as a bioreactor that engineers the cells by reproducing the biomimetic stimuli, both dynamic mechanical cues and chemical cues, to the micro-engineered tissues. Conventional 2D flat and simple environments poorly reflect the key elements of an actual body, (e.g., 3D arrangement, softness, elasticity, mechanical stimuli, fluid flow, and extremely diverse communications) [54-61]. Accordingly, 3D model platforms have been developed to overcome the limitation of 2D cultures in biological and pharmaceutical applications. AM techniques with biological materials have the potential to generate complex 3D constructs that more closely recapitulate the complexity and heterogeneity of tissues and organs.
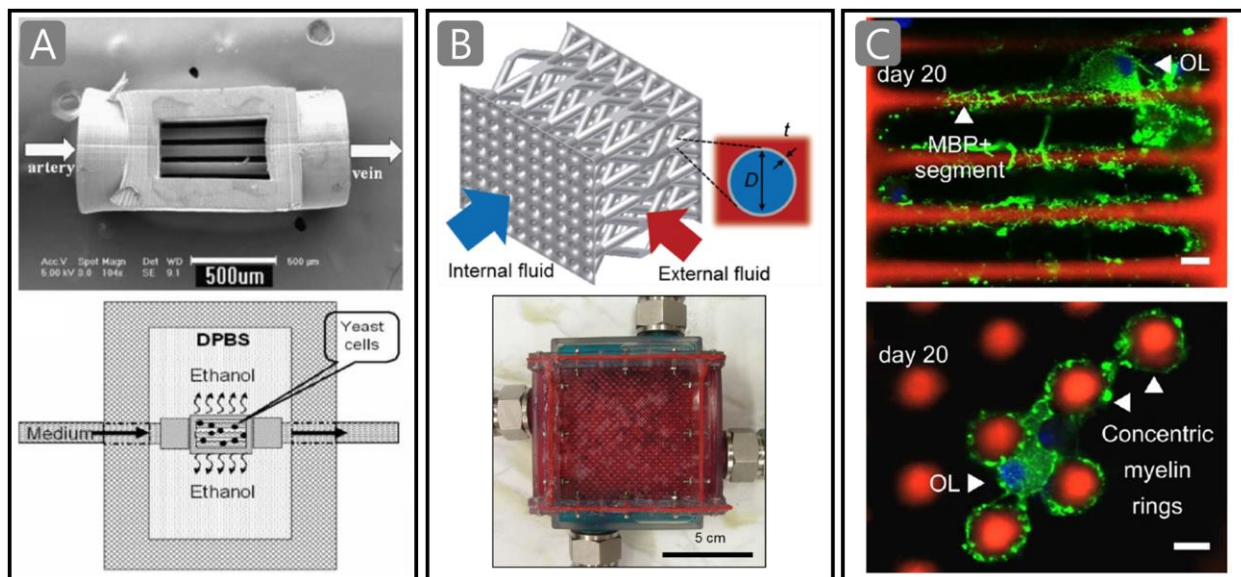

Figure 8. (A) 3D microbioreactor for yeast cell culture. Reprinted from reference [54] with permission. (B) 3D bicontinuous fluid networks for heat and mass exchange. Reprinted from reference [55] with permission. (C) 3D-printed artificial cells that form the myelin sheath. Reprinted from reference [56] with permission.

Fang et al. presented a DLP-printed 3D microbioreactor to enhance the mass transport in cell culture (Fig. 8A) [54]. These microfabricated bioreactors showed a regulation of metabolism and the growth of yeast cells by controlling the density of the micro-capillaries. The 3D microbioreactor had two ports for the

injection needle cannulated flow, a series of 40 µm-diameter capillaries, and an open wall to allow cell seeding. They also demonstrated 3D branching fluidic microarchitectures built without flow cannulation points.

Roper et al. presented a scalable approach to printing 3D bicontinuous fluid networks with thin-walled interfaces, enabling a polymer heat exchanger toward artificial organs (Fig. 8B) [55]. These 3D bicontinuous fluid networks were implemented by the fabrication of sacrificial polymeric scaffolds via DLP or SPPW, conformal coating with parylene, and then selective removal of a sacrificial scaffold. AM with the conformal coating method enabled an efficient bicontinuous fluidic network with prime surfaces and allowed the use of interface materials to be selected for multifunctional properties such as electrical conductivity, antifouling ability, and density. Furthermore, this approach opened up a new possibility for biological heat and mass exchange systems toward artificial organs, including artificial lungs, with similar overall size to natural organs.

Creating very soft 3D constructs, which match the brain tissue, and are still able to withstand the pressure of adherent cells, has been particularly challenging. In brain tissue engineering, super soft 2D gels mimicking the brain tissue differentiated into neurons has not been not able to visualize the myelin formation in-vitro. Van Vliet et al. recently demonstrated an engineered artificial axon printed through the DLP and DIW methods, which was completed with axons around which the oligodendrocytes could grow (Fig. 8C) [56]. The thin, self-holding, soft fibers had extremely low stiffness, but remained freestanding such that the oligodendrocytes cells could wrap the myelin membranes around it.

The advancements in additive biofabrication techniques have led to the construction of complex organ-on-a-chip devices with a modular design and an advanced microfluidic system. 3D-printed organs-on-a-chip have come into the spotlight with their capability to replicate organ-level functions by introducing cells into a microfluidic device that includes precisely fabricated chambers and channels. Chen et al. demonstrated cell-printed livers-on-chips by DLP-based 3D bioprinting (Fig. 9A) [57]. They fabricated the liver unit, which is a lobule structure, by using two bio-inks of the 5% GelMA (~5 kPa compressive stiffness similar to a healthy liver tissue) for the parenchymal tissue formation and the 25% GelMA/1% glycidal methacrylate-hyaluronic acid (~4 kPa compressive stiffness) for vascularization. They also generated a hexagonal liver lobule with a complex pattern that is composed of two parts, namely the parenchymal tissue part of the human-induced pluripotent stem cell-derived hepatic progenitor cells and the non-parenchymal tissue part with a radial structure of the supporting cells. This approach enables the development of a 3D biomimetic liver model that recapitulates the native liver module architecture for early drug screening and disease modeling. Sun et al. printed an artificial human cervical cancer with a porous 3D architecture to ensure the oxygen supply [58]. They extruded the fibrinogen-gelatin-alginate biological ink containing human cervical cancer cells (Hela) in a lattice pattern and observed the realistic morphological changes. The 3D-printed Hela cells showed a higher proliferation rate in the 3D microenvironment and tended to form cellular spheroids. These printed 3D tumor models can provide a useful toolbox for the evolution of 3D cancer study. Jiang et al. reported another strategy for the integration of electrospun membranes into organ-on-a-chip platforms (Fig. 9B) [59]. The printed electrospun membrane was adopted as the solid substrate and sandwiched between two slabs of polydimethylsiloxane (PDMS)-enclosed microchannels. The printed device was demonstrated to improve the sensitivity and the signal-to-noise ratio of the microfluidic immunoassay for HIV as compared to the commercially available track-etched polycarbonate membrane. Compared with other methods, this approach is simple, cost-effective, and easily scaled up to areas of 5 cm × 5 cm, thereby enabling usage in conventional immunoassays in microtiter plates as well. Cho et al. introduced a novel AM approach with multiple nozzles that enabled the simultaneous printing of biomaterials and non-biomaterials for organ-on-a-chip applications (Fig. 9C) [60]. The liver was selected

for their platform evaluation. The results showed a significant enhancement of the liver function of the liver-on-a-chip. Less protein absorption was obtained compared to the PDMS platform. They also observed a one-step fabrication of an organ-on-a-chip without a secondary cell-seeding process. This AM method can be applied for various organ-on-a-chip applications with proper microreactor design and material selection, and will provide a new paradigm in the field of organ-on-chip development.
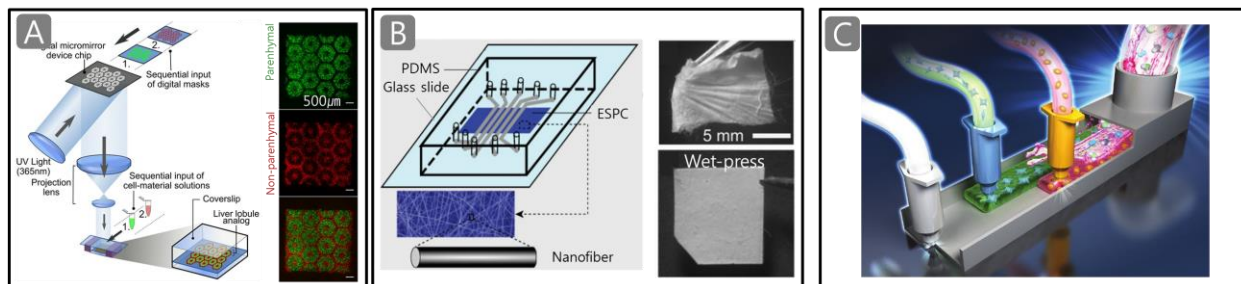

Figure 9. Complex organ-on-a-chip devices. (A) DLP-printed livers-on-chips. Reprinted from reference [57] with permission. (B) Electrospinning-printed microfluidic chip devices Reprinted from reference [59] with permission. (D) One-step and multimaterial printing of organ-on-a-chip. Reprinted from reference [60] with permission.

3.3 Microarchitected reactors for energy applications

The research interest in the use of AM technologies for electrochemical energy conversion and storage applications has continued to gain momentum in the recent years [62-71]. AM has advantages to employ in electrocatalysis as a method of rapidly producing and iterating prototype designs. Figure 10 summarizes some representative examples of the prototype 3D-printed electrocatalytic reactors.
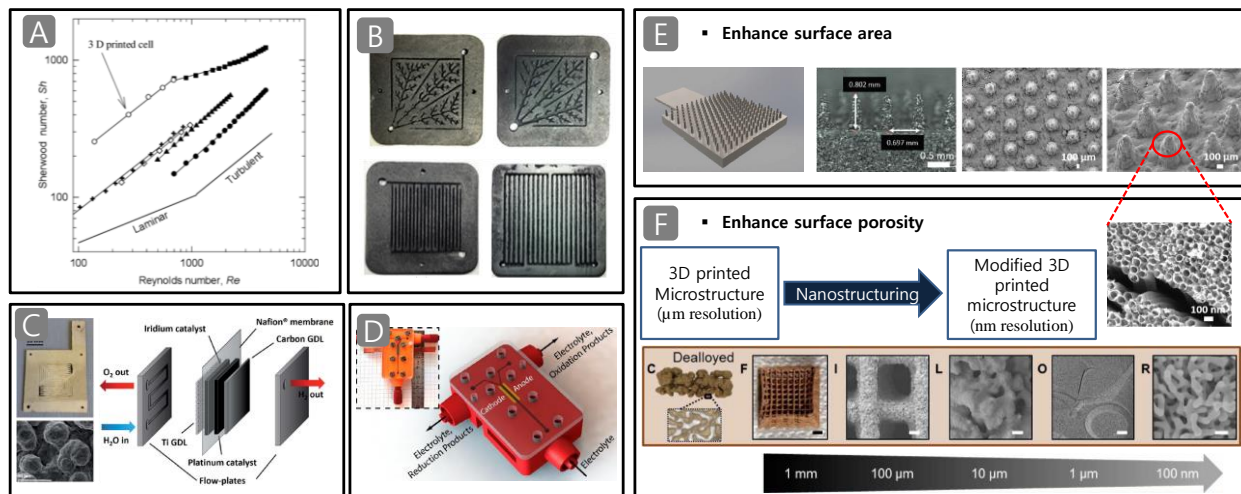

Figure 10. Examples of additive manufactured electrocatalytic devices. (A) 3D-printed polymeric electrochemical devices. Reprinted from reference [62] with permission. (B) Interdigitated bio-inspired graphite composite plate channels. Reprinted from reference [63] with permission. (C) Polymer electrolyte membrane electrolyzers with Ag coated on polypropylene. Reprinted from reference [64] with permission. (D) SLA-printed membrane-free electrolysis cell. Reprinted from reference [65] with permission. (E) 3D conical arrays of the TiO_2 electrodes for the photoelectrochemical reaction. Reprinted from reference [66] with permission. (F) 3D hierarchical catalytic architectures. Reprinted from reference [67] with permission.

Ponce de Leon et al. investigated a 3D flow reactor cell printed with ABS and nickel electrodes (Fig. 10A) [62]. The 3D-printed cell showed a turbulent flow at a low Reynolds numbers because of the

16

electrolyte channel geometry. The further optimum design of cells was proposed based on the evaluated mass transport behavior. In another example, a bio-inspired flow reactor design inspired by the venation structure of a tree leaf was developed with SLS-printed graphite-composite plates (Fig. 10B). Numerical and experimental studies were performed to investigate the transport efficiency of the bio-inspired reactor design. The results showed a substantial improvement of the fuel cell performance by 20-25% compared to the conventional designs [63]. Cronin et al. also demonstrated another prototype of FDM-printed microreactor device, namely a proton-exchange membrane (PEM)-based water electrolyzer (Fig. 10C) [64]. They presented a low-cost construction of a lightweight electrolyzer with an integrated PEM and reported a high energy efficiency of 86.48% at 2 A cm^{-2} and 80 °C. The potential of the lightweight and cheap electrolyzers will include the other electrochemical devices, such as flow batteries and fuel cells. Hashemi et al. recently reported on SLA-printed electrochemical reactors to develop a membrane-less electrolyzer that enables high-throughput and smooth surfaces for precise flow conditioning (Fig. 10D) [65]. They demonstrated that the developed membrane-less reactor containing more efficient catalysts can provide a higher throughput than its microfluidic counterpart and open up a new possibility for the realization of cost-effective and scalable electrochemical reactors toward the renewable energy sector.

Additional post-processing strategies are sometimes required to enhance the electrochemical performance of 3D-printed electrocatalytic reactors because the 3D porous electrodes with an enhanced surface area are desirable for further increasing the electrochemically active area. As an example of the post-treatment, Wallace et al. explored the feasibility of metal-based SLS-printed electrode arrays for the photo-driven electrochemical catalytic water splitting. The electrode arrays were further enhanced by the direct growth of TiO_2 nanotubes on the 3D-printed Ti surfaces [66]. While the initial printed features were sub-mm, anodization allowed for further increasing of the active catalytic surface area by several orders of magnitude (Fig. 10E). In addition, Biener et al. recently reported 3D hierarchical nanoporous gold with engineered microarchitectures by combining DIW printing and the dealloying process (Fig. 10F) [67]. These hierarchical structures showed a large surface area, a high electrical conductivity, and a low-pressure drop, resulting in enhanced mass transport and reaction rates for both liquids and gases.

In a continuous-flow microreactor operation, the heterogeneous structured catalytic material is desirable for an easier work-up and an efficient chemical transformation [8]. The monolithic architecture used in car catalytic converters is the most well-known example of a common structured catalytic material (Fig. 11A) [72]. The many mm-sized (or sub-mm) parallel channels in monoliths enable high gas or liquid flow rates with low pressure drops. A large pressure drop over a car exhaust catalytic converter would increase the fuel consumption by several percent. With that said, the fluidic transport with the low-pressure drop is one of the most important benefits of the monolithic reactors. However, a laminar flow is developed inside the monolith channel because of its small size, which results in relatively poor transfer conditions within the catalytic reactors. Therefore, the diffusion is dominant in the mass transfer of reactants (i.e., transport from the gas or liquid phase to the catalytically active channel wall). Accordingly, ~ 90% of the exhaust emissions is converted after passing through the first ~ 10% of the monolith length because of the high flow rates of reactants and slow diffusion of remaining low concentration of pollutants. In addressing this issue, the monolith length is usually increased, thereby resulting in it occupying more space and requiring more of the expensive catalytic materials. Reducing the channel size in the monoliths (i.e., increasing the monolith density) would reduce the reactant diffusion path, but would simultaneously lead to an increased pressure drop. Thus, the efficient utilization of precious metal catalysts and removal of the last pollutants in the catalytic reactor are becoming a more important issues when considering more strict emission regulations [73].

The promising approach to enhancing mass transfer is based on the introduction of a 3D microarchitecture to transform the laminar to turbulence flow and promote transverse mixing by cross-connected structures. However, most catalytic supports have not been able to obtain complex 3D geometries because of the limitation of the traditional manufacturing methods, such as extrusion.
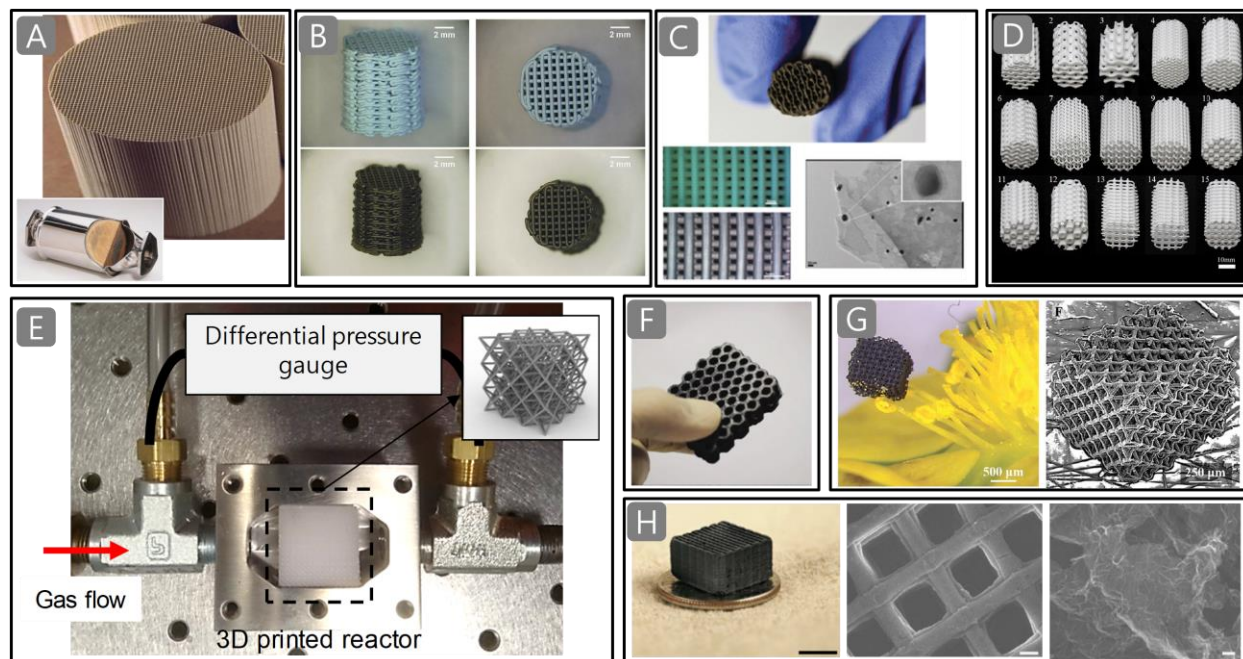

Figure 11. (A) Conventional ceramic monoliths for catalytic converters [72], (B) DIW-printed alumina supports with Cu-based catalysts [74], (C) 3D NiMo/PVA catalytic structures for process intensification [75], (D) DLP-printed catalytic ceramic substrates [76], (E) Small-scale test setup of 3D-printed lightweight ceramic microlattice for low-heat capacity reactors [S. Kim et al., unpublished], (F) 3D-printed Pd/C monolithic catalyst [77], (G) DLP-printed microarchitected graphene aerogels [78], (H) DIW-printed graphene aerogel microlattices [79].

Here, the advancement of AM methods has enabled the shaping of 3D catalytic supports to improve the mass and heat transfer characteristics. Gil et al. demonstrated the DIW-printed catalyst-immobilized ceramic support for a metal/oxide heterogeneous catalytic system. They prepared an aqueous colloidal gel ink based on a mixture of alumina ceramic powder, polymer binders, and $Cu(NO_3)_2$. (Fig. 11B) [74]. After sintering the 3D woodpile porous structures, Cu/Al_2O_3 catalyst-ceramic supports were obtained with a high mechanical strength, a high surface-to-volume ratio, and a controlled porosity (Fig. 11B). The resulting 3D ceramic support showed high catalytic efficiency and good recyclability in different Ullmann-type coupling reactions for the C-N bond formation. Another type of DIW-printed intensified catalytic reactors was reported by Beltramini et al. They developed a printable composition of $NiMoO_2$, water-soluble PVA, and starch. Even though the as-printed structures lost 70% of its initial weight during subsequent pyrolysis, its geometry is maintained because of uniform shrinkage. A 3D carbon scaffold with catalyst-loaded carbon containing up to 25 wt.% was tested in CO conversion at high feed flow rates (Fig. 11C) [75]. Ortona et al. investigated the effect of exhibited topology on the mechanical and flow properties of new and novel architected catalytic substrates (Fig. 11D) [76]. They proposed architected and controllable topologies based on the minimal surface framework as catalytic substrates. After DLP printing with a photocurable ceramic composite material, they focused on studying the mechanical and fluidic properties of the printed structures toward catalytic ceramic substrates. Both numerical simulation and experimental test showed

that a triply periodic minimal surface substrate exhibited the highest mechanical properties and the least pressure drop among the tested substrates.

In addition to the improvements mentioned above, one approach, currently under development in our lab, has been studied to improve thermal response of 3D ceramic substrates to alleviate cold-start emission [S. Kim et al., unpublished]. Catalytic conversion efficiency largely depends on the temperature of the constituent substrate and its thermal response. However, most of the conventional catalytic converters with a slow thermal response, they cause cold-start problems which lead to excessive pollutant exhaust due to low conversion efficiency. The key idea of achieving efficient catalytic substrates is leveraging on the geometrical benefits of 3D microlattices of thin walled hollow-tubes realized through AM processes. In the preliminary test (Fig. 11E), we have found the fast-thermal response and flow redistribution of working fluids inside 3D ceramic microlattices compared to the conventional ceramic monolith structure.

Moreover, Liu et al. recently demonstrated a carbon-based 3D catalytic system was achieved with the carbonization of thermosetting resins (Fig. 11F) [77]. The carbon macrostructure was printed through the DIW method, and Palladium (Pd) was then loaded on the printed structures. The Pd/C 3D structures were tested for the catalytic combustion of methane. Consequently, the Pd/C reactors showed an enhanced catalytic performance, indicating that they can serve as efficient catalytic materials for industrial applications. Carbon materials have been intensively studied as catalytic materials because of their inherent advantages, such as high surface areas, good electrical conductivities, and chemical stabilities. Many different carbon structures from nanoscale to macroscale have been used to improve catalytic performances. The fabrication of carbon-based architected reactors is becoming more accessible with the help of AM techniques. However, most 3D graphene foams exhibit a significant degradation of mechanical properties. To alleviate this issue, Zheng and Worsley developed a light-based AM process to create hierarchical microarchitected graphene structures with an arbitrary complexity, showing enhanced mechanical properties at a decreasing density (Fig. 11G) [78]. The AM technique enables the obtainment of order-of-magnitude finer features and opens up new possibilities for future graphene applications, including energy storage and conversion, and catalytic reactor. Further, Worsley et al. also reported compressible 3D periodic graphene aerogel microlattices for a broad range of applications, such as graphene-based electronics, energy storage devices, and catalytic scaffolds (Fig. 11H) [79]. They demonstrated the DIW-printed periodic graphene aerogel microlattices that were lightweight and highly conductive and exhibited super compressibility (i.e., up to 90% compressive strain). Adapting AM technologies to graphene aerogels can realize the fabrication of a complex aerogel architecture for a promising catalytic material.

3.4 Battery reactor and photomicroreactor

A 3D microbattery was identified as a novel design approach to deliver improved areal energy density while maintaining good power and cycling performance. However, energy storing reactions, especially multielectron reactions are still difficult to achieve with micron-sized structured battery materials [80]. Batteries and electrochemical capacitors consisting of two electrodes and one electrolyte exhibit performances that can be improved by utilizing structured porous electrodes because of their shorter diffusion length, smaller ionic transport resistance, and increased surface area. Thus, the ability of AM to fabricate 3D structures with microscale dimensions can be of great benefit in 3D electrode architectures.

For instance, the developed 3D microarchitected electrodes of a lithium (Li)-based battery showed great potential in achieving high power and energy densities. Lewis et al. demonstrated DIW-printed 3D interdigitated microbattery architectures (3D-IMA) composed of lithium titanium oxide (LTO) and lithium iron phosphate (LFP), which serve as anode and cathode materials, respectively. The concentrated LFP and LTO inks enabled the printing of thin-walled (~ 30 µm) anode and cathode structures. This 3D IMA

exhibited a high areal energy density of 9.7 J cm^{-2} at a power density of 2.7 mW cm^{-2} (Fig. 12A) [81]. Another promising prototype is the 3D microlattice electrodes with porous solid struts are fabricated by direct aerosol jetting of silver (Ag) nanoparticles (Fig. 12B) [82]. Park and Panat reported that these complex and controlled 3D electrode architectures led to a significant improvement in the battery performance (e.g., 400% increase in specific capacity, 100% increase in the areal capacity compared to a thin solid Ag flat electrode). These results indicate that a hierarchical structure of the 3D microlattice architectures enables the enhancement of the electrolyte transport through the porous electrodes and increases the accessible surface area for the electrochemical reaction.

However, these two DIW-based AM methods suffer from an inherently low throughput (i.e., low delivery rate). As one of the alternative methods for overcoming this limitation toward a large-area and high-throughput fabrication, other AM methods (e.g., SPPW) have been used to develop microlattices for the microarchitected battery reactor application. Xu et al. developed a hollow Au microlattice as positive electrodes for Li–O^2 batteries by initially fabricating an architected polymeric scaffold by the SPPW, followed by depositing a thin Au layer through sputtering and electrodeposition prior to chemical etching to remove the polymer (Fig. 12C) [83]. The experimental results showed that 3D microlattices may provide enabling mechanical robustness and enhance the surface area over a factor of 30 compared with a thin film with the same footprint.
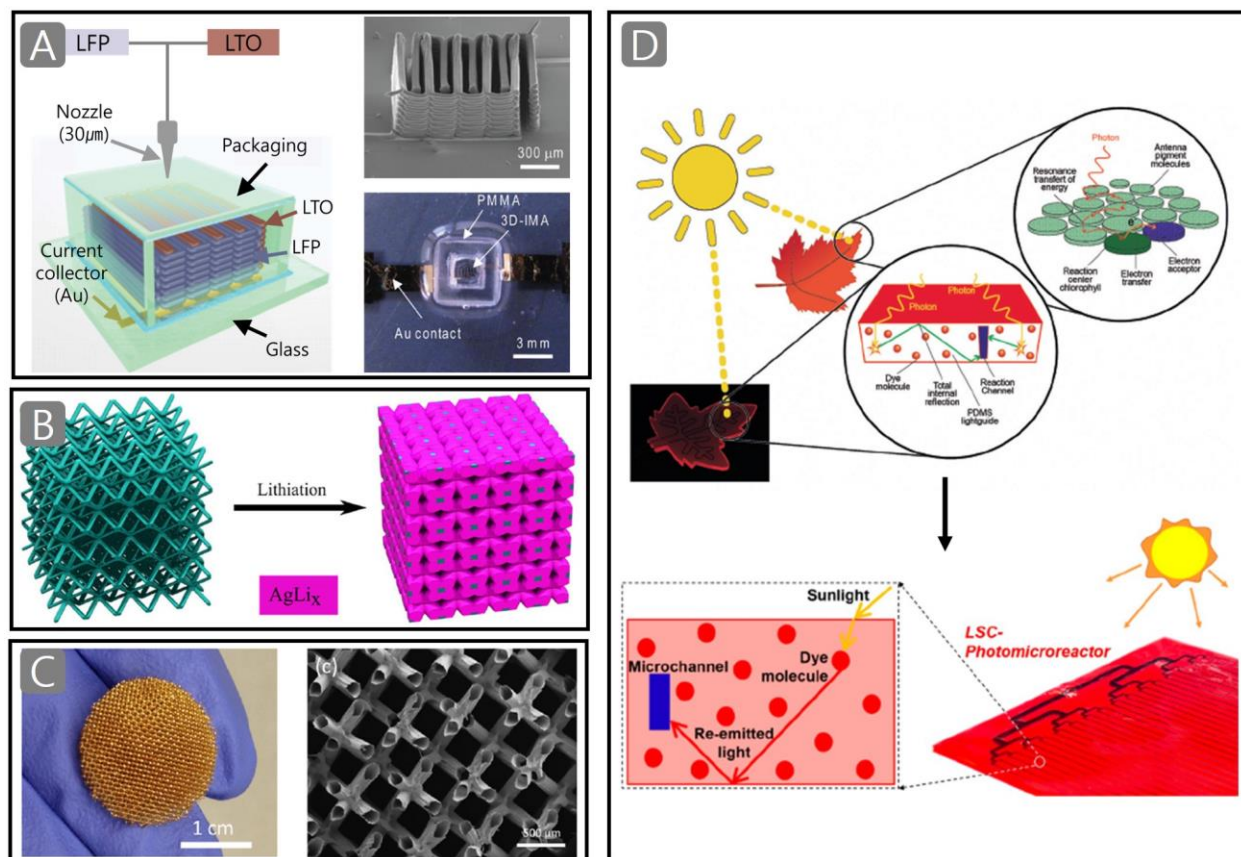

Figure 12. (A) DIW-printed Li-ion microbattery reactor [81], (B) Direct aerogel jetting-printed Li-ion microlattice batteries, [82]. (C) SPPW-printed Li-O$_2$ Batteries (Left: optical image of a 3D hollow Au microlattice battery electrode; right: SEM image of the hollow microlattice) [83], (D) 3D-printed luminescent solar concentrator-photomicroreactor (LSC-PM) [84-85].

More interestingly, with the combining effect of the microreactor and AM technologies, significant effort has been devoted to developing a wide variety of energy-efficient continuous-flow photochemistry. Luminescent solar concentrators (LSC) are glass or polymeric slabs doped with a luminophore, (i.e., generally, a fluorescent dye). The photons absorbed by the dye are reemitted via fluorescence and have a high probability of being trapped in the slab due to total internal reflection [84]. Therefore, the whole slab acts therefore as a light guide. When a flow microreactor is integrated into this design, the photons generated in the LSC can be used to power a photochemical reaction (Fig. 12D) [84]. Nöel et al. introduced a leaf-inspired LSC-photomicroreactor (LSC-PM) that constitutes a merger between LSC and a flow microreactor to enable efficient photochemical reactions powered by solar irradiation. The first LSC-PM device was based on fluorescent dye-doped PDMS, and was used to collect sunlight, focus the energy to a narrow wavelength region, and transport that energy to embedded microchannels, where the flowing reactants are converted. FDM-printed LSC-PMs were then demonstrated for scale-up (Fig.12D) [85]. The AM method helped to rapidly produce different prototypes and optimized key design parameters, including the inter channel spacing, which is an important parameter for the scaling up of LSC-PMs.

4. Perspectives and outlook

A tremendous potential in the field of functional microreactor technology field has been observed with the steady increase of the impact of AM technologies along with functional materials. The rapid interaction between digital data and substantial objects, inherent to a digital fabrication flow, will be of increasing value in streamlining both research and manufacture of reactors with structured materials. The interaction between AM and digital design is a critical enabling approach for the rapid and versatile fabrication of efficient MAR. We envision a future where the AM microreactor technologies and processes are fully integrated into various energy, environmental, and biological applications. However, despite the encouraging future of AM technologies, the challenges and research opportunities as regards extending the range of printable functional materials, low throughput, and low feature resolution remain prior to the broad implementation of this paradigm.

4.1 Challenges

Material development and multifunctionality: A limited number of available materials can be processed via AM methods, which are mainly restricted to polymers, certain metals and alloys, or ceramics. The design framework begins with the selection of the AM methods and the related material library based on the given functional requirements. Although AM technologies have shown great potential in fabricating multifunctional structures, an important challenge for the AM methods is their limitation in functional materials [16, 86]. Considering the diversity of functional materials, AM with functional materials is critical in elevating its impact in the microreactor and material societies. The capability to fabricate functional materials in 3D can provide new functionalities beyond the materials themselves if they are well designed into specific geometries. In addition, the multifunctionality of a designed component usually requires using multimaterial AM processes. Thus, multimaterial AM methods for multifunctional MARs should control and optimize localized material properties of fabricated 3D structures with voxel-by-voxel (a voxel is defined by a physical object of a collection of finite volume elements). However, the current multimaterial AM capability is not sufficient for voxel-by-voxel printing due to the limited frequency and channels of multiple material exchange. In addition, the spatial resolution of multimaterial AM processes is restricted by material blur occurred in the adjacent regions of different 3D-printed materials. For example, the printed material property (e.g., biocompatibility and/or biotoxicity) is specifically a critical challenge in biological

21

MAR. While many materials have been combined to recapitulate the critical properties of actual biological objects, they often fail to capture the full geometrical complexity and physiological functionality of the original tissue/organs. Furthermore, the fabrication of biological architectures that match the mechanical properties of the target tissue, cell, or scaffolds remains difficult. Therefore, the interaction between the selected material and the target biological applications must be considered, which can limit the choice of printable materials. The use of multiple materials of functional MAR in this review is based on either the starting materials are pre-mixed or composited prior to the AM process, or the second material is integrated by infiltration, impregnation, coating or other post-processing techniques. In the future, more new functional materials must be explored and incorporated into printed 3D structures to achieve multifunctional properties (e.g., ceramics with mechanical rigidity, scaffolds with bio-degradability, and nanocomposites for chemical or thermal resistance) toward advanced chemical/catalytic MAR and energy MAR.

Scalable and multiscale AM: With the context of the scaling issue described in Section 2.1.4, most of the existing AM methods can only fabricate 3D structures with a uniform resolution (d) and delivery rate (P) (Fig. 3). However, the functional devices are desirable to contain both micro- and/or nanoscale features (i.e., multiscale) or range from dozens of centimeters to several microns (i.e., scalable) [86]. The existing AM methods can hardly fabricate such a complex geometric shape, produce the functional performance of the built scalable and multiscale 3D objects. Therefore, the integration of printed parts at different dimensional scales and different materials is one of the major challenges that must be addressed before these AM technologies and materials can extend their applications in multiple fields.

Incompatibility of conventional STL format for design and modeling scale-up: Advancements in the AM methods have led to increasing resolution and print volume; thus, another important challenge as regards CAD software and STL format. Majority of the available CAD software are suited for conventional manufacturing processes, such as extrusion, lofts, and revolves, and are not capable of generating complex multiscale structures and specifying multiple material variations within an object. In addition, the STL file format has not changed in three decades, and will become a limiting factor in describing complex shape and topology because of the large STL file size for such parts. An STL file is basically a list specifying all the triangular faces that make up an object, with each triangular face defined by the 3D-coordinates of its three vertices. This is a limitation because a STL file can quickly grow from 500 MB to several GBs in size when a large order-of-magnitude difference exists in the minimal feature size and the volume of an object. For example, hierarchical designs with the orders of magnitude in the feature size and the span of multiscale creates difficulty with the STL format by requiring a large memory during modeling and producing large files after exports. The STL file format is no longer suitable for high-resolution and large-scale objects because it needs to list every single vertex of a triangular mesh over the object surface. The development of another file format is required to address this challenge for multiscale and complex objects.

4.2 Opportunities

Many opportunities that will accelerate the AM of functional MAR. This field will be enhanced by further cross-disciplinary advances in each of the AM technologies, materials, and digital design.

Multimaterial printing toward multifunctional reactor devices: Multimaterial AM is a term classified as a process, in which different materials or chemicals are physically delivered to any spatial location in 3D during additive manufacturing and where compositional variation can be freely controlled by a computer and a program [87]. The ability for the multimaterial AM technique is essential for multifunctional microreactor applications. Recently, some methods in DIW [60, 88], DLP [18, 106], and TPL [89] are capable of multimaterial printing from multiple materials. Another possibility which is

complementary with the multiple materials approach is to use only a single material throughout the entire AM process, but change a suitable stimulus during the printing. In response to the proper stimulus, the material properties may change, leading to the possibility of many different material properties from a single material. Conceivable stimuli that might be adjusted include power, wavelength or polarization of light or the strength and direction of an electric field or magnetic field.

Furthermore, Vaezi et al. suggested hybrid AM methods being combined within the same machine that is capable of fabricating multifunctional 3D structures in a sequential layer-by-layer process that combines mechanical, chemical, thermal, electronic, and other functions in a single component [87]. MacDonald and Wicker also introduced a major opportunity of multiprocess (or hybrid) 3D printing for fabricating of multifunctional structures with multiple materials, in which complementary processes, both novel and traditional, are combined to advance the future of manufacturing [90]. This hybrid AM strategy with complementary processes may provide spatial control of multiple materials, geometry, and functionality. Ahn et al. also suggested a hybrid 3D printing process consisting of aerodynamically focused nanoparticle (AFN) printing, micromachining, and focused ion beam milling, and spin-coating (Fig. 13A-i) [91-93]. This hybrid process showed the potential to overcome the limitations of individual techniques by enabling improved scaling, dimensional degree of freedom, and high-resolution down to ~ 50 nm. Kim et al. recently demonstrated the hybrid AM method combined with light-based and material deposition-based printing (Fig. 13A-ii) [94]. This multiprocess (or hybrid) approach can also provide the capability of fabricating multiscale structures by the integration of multiple AM processes. However, the hybrid approach can only adapt to building multiscale objects with a special design. How to integrate different AM processes to fabricate 3D objects with any universal design still remains a substantial challenge.

Machine learning: Another opportunity can exist in adapting advances in machine learning to improve the design of a functional MAR or hybrid AM processes. Machine learning techniques can be applied to various machining processes to improve product quality and rates, to monitor the health of systems, and to optimize the design and process parameters [95]. The processing parameters of AM can exert a huge impact on the printed microstructure and on the performance of the subsequent products; therefore, they are critical for building a process-structure-property-performance relationship for AM. Considering the large dataset that is currently available, the strong computational power, and the sophisticated algorithm architecture, machine learning techniques can help in several aspects of AM, including model design, in-situ monitoring, and quality evaluation, instead of traditional numerical and analytical models [96]. Zare et al. reported that machine learning could be employed to optimize the chemical reactions in microreactors (Fig. 13B) [97]. By iteratively recording the results of a chemical reaction and selecting new experimental conditions to improve the reaction outcome, their model showed superior performance by using 71% fewer steps on both simulations and real reactions, thereby demonstrating its capability of speeding up reaction optimization. The recent advancements in machine learning have increasingly been used in multiple engineering fields. Engineers and researchers utilize higher-level computational methods to help leverage the massive data streams of their findings for real-world applications. We envision that the benefits of machine learning in engineering are vast and have completely changed the research arena.

Multi-interaction (responsive) microreactor system: Advances of AM technologies and printable functional materials can provide additively embedded sensors or communication functions into MAR, enabling a data acquisition in-situ and a continuous interaction mode to operate multiple-reactor platforms. Lewis and Parker recently have made an entirely 3D-printed heart-on-a-chip device with an integrated sensor to measure the contractile strength of the tissue [88]. Using DIW, they deposited six specialized inks to form a detachable sheet that folds upward upon cardiomyocytes contraction. The sensor

layer consists of a strain gauge wire printed with a thermoplastic polyurethane ink. A mechanical model was needed to precisely convert the measured resistance signals to the generated stresses by the tissues. An automated and DIW-printed heart-on-a-chip device allows researchers to easily collect reliable data for short-term and long-term studies. This approach to building organs-on-chips not only allows us to easily change and customize the design of the system, but also drastically simplifies data acquisition. Microfluidic reactor technologies enable the integration of multiple organ-on-chips in a single analytic system to simulate the dynamic organ-organ interactions in a living body. The multiple fluidic interconnections for organ-on-chips developed by Griffith et al. [98] has been used to construct a multi-microreactor platform by adopting sophisticated recirculation architectures that better mimic the blood circulation and achieve a differential flow distribution toward different organ models (Fig. 13C). The configurability of the multi-reactor platform relies on an array of individually addressable micropumps in-line with microchannels that are integrated in a single device. This multi-interaction system is especially helpful during the development stage of multiorgan microfluidic platforms because one can modify the collection of organ models to include and adjust the fluidic parameters (e.g., flow rates and flow distribution) without reinventing the whole system. This sensing embedded and interacting system allows devices to become autonomously to communicate their state and the state of their environments to the surrounding systems. Such a communication ability would allow for the further integration of the device into advanced software systems, and may lead to dynamic and smart microreactor systems.

Parallel and roll-to-roll process toward an economical, scalable AM process: Most of all, the low printing throughput compared to silicon-based or machining-based subtractive manufacturing hinders the adaptation of these AM techniques for the production of functional microreactors in the industry. However, the trade-off between the throughput and the feature resolution will always exist in both 2D and 3D manufacturing by following the universal trend of miniaturization [99]. We envision that the improvement of the printing throughput can potentially be achieved using multiple nozzles [100], beams [2, 101], images [28-29], or lenses for parallel printing (Fig. 13D). In addition, the high-throughput and cost-efficient processing of printable materials using continuous processes, such as roll-to-roll (R2R) [102-105] are of great importance for their future adoption in the industrialization of AM methods (Fig. 13E). The R2R process is a well-established process with applications ranging from commercial printing to large-area electronics, photovoltaics, advanced functional devices, such as lighting, and sensors. Although the implementation of R2R on 3D structures has still remained as a critical challenge, we anticipate that the R2R process can be one of the promising tools for high-throughput, scalable AM printing in the near future.
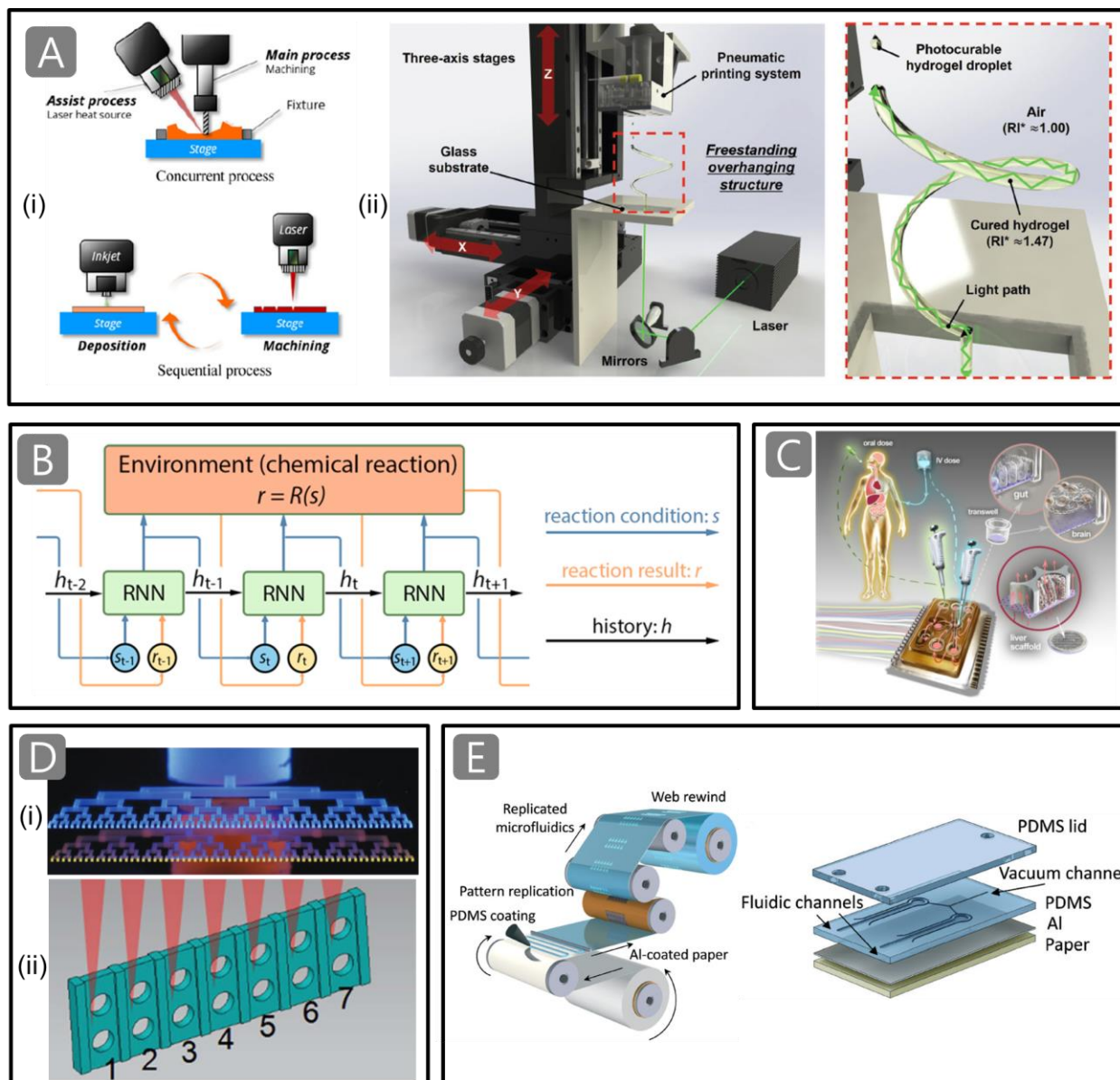
Figure 13. Future opportunities for additively manufactured functional microreactors. (A) Hybrid AM process of 3D constructs [91,94], (B) Machine learning to optimize chemical reactions [97], (C) Multi-microreactor platform for interconnected microphysiological systems [98], (D) Parallel AM printing system for high-throughput [i: [100]; ii: [101]], (E) Roll-to-roll replicated PDMS microfluidics on an Al-coated paper [105].

In summary, the present and future impacts of AM technologies in the field of functional microreactor are undeniable. Nonetheless, from the abovementioned discussions, the scope of improvement that must be achieved is vast in order to extend their applications. Cross-disciplinary teams that transform the way we design and implement functional microreactors should be essential in addressing several challenges opportunities before AM technologies amplify their impact in diverse aspects of today's industry. Many research groups are currently exploiting the AM capabilities to meet the ever-changing needs for high-performance functional microreactor devices. For the future, we envision that a more collaborative and interdisciplinary efforts would lead to the ongoing development of new design methodologies for

integrating the state-of-the-art AM technologies and materials to enable the improved performance through devices and products, maximizing the impact on the community.

Acknowledgements

References

1. Ehrfeld, W., Hessel, V., and Lowe, H. (2000) Microreactors : new technology for modern chemistry. *Weinheim, WILEY-VCH Verlag GmbH.*

2 . Yazdi, A., A., Popma, A., Wong, W., Nguyenm T., Pan, Y., and Xu, J. (2016). 3D printing: an emerging tool for novel microfluidics and lab-on-a-chip applications. *Microfluid Nanofluid* 20(3): 50.

3. Ikuta, K., Maruo, S., Fujisawa, T., and Tamada, (1999). A. Micro concentrator with opto-sense micro reactor for biochemical IC chip family. 3D composite structure and experimental verification. *International Workshop on Micro Electro Mechanical Systems*, MEMS 12, 376-381.

4. Ikuta, K., Ogata, T., Tsubio, M., and Kojima, S. (1996). Development of mass productive micro stereo lithography (Mass-IH process*). Proceedings of Ninth International Workshop on Micro Electromechanical Systems*, 301-306.

5. Ikuta, K., Hirowatari, K., and Ogata, T. (1994). Three dimensional micro integrated fluid systems (MIFS) fabricated by stereo lithography. *Proceedings IEEE Micro Electro Mechanical Systems An Investigation of Micro Structures, Sensors, Actuators, Machines and Robotic Systems*, 1-6.

6. Ikuta, K., Maruo, T., Fukaya, Y., and Fujisawa, T. (1998). Biochemical IC chip toward cell free DNA protein synthesis. *Proceedings MEMS 98. IEEE. Eleventh Annual International Workshop on Micro Electro Mechanical Systems. An Investigation of Micro Structures, Sensors, Actuators, Machines and Systems*, 98CH36176, 131-136.

7. Teh, K., S. (2017). Additive direct-write microfabrication for MEMS: A review. *Frontiers of Mechanical Enginerring*, 12(4), 490-509.

8. Parra-Cabrera, C., Achille, C., Kuhn, S., and Ameloot, R. (2018). 3D printing in chemical engineering and catalytic technology: structured catalysts, mixers and reactors. *Chemical Society Reviews*, 47(1), 209-230.

9. Surjadi, J. U., Gao, L., Du, H., Li, X., Xiong, X., Fang, N. X., et al. (2019) Mechanical Metamaterials and Their Engineering Applications. *Advanced Engineering Materials*, 21(3), 1800864.

10. Parra-Cabrera, C., Achille, C., Kuhn, S., and Ameloot, R. (2018). 3D printing in chemical engineering and catalytic technology: structured catalysts, mixers and reactors. *Chemical Society Reviews*, 47(1), 209-230.

11. Moroni, L., Boland, T., Burdick, J. A., Maria, C., Derby, B., Forgacs, C., et al. (2018) Biofabrication: A Guide to Technology and Terminology. *Trends in Biotechnology*, 36(4), 384-402.

12. Simpson, R. L., Wiria, F. E., Amis, A. A., Chua, C. K., Leong, K. F., Hansen, U. N., Chandrasekaran, M. and Lee, M. W. (2008). Development of a 95/5 poly (L-lactide-co-glycolide)/hydroxylapatite and β-tricalcium phosphate scaffold as bone replacement material via selective laser sintering. *Journal of Biomedical Materials Research Part B: Applied Biomaterials*, 84(1), 17-25.

13. Zhou, W. Y., Lee, S. H., Wang, M., Cheung, W. L., and Ip, W. Y. (2008). Selective laser sintering of porous tissue engineering scaffolds from poly (L-lactide)/carbonated hydroxyapatite nanocomposite microspheres. *Journal of Materials Science: Materials in Medicine*, 19(7), 2535-2540.

14. Wang, Z., Abdulla, R., Parker, B., Samanipour, R., Ghosh, S., and Kim, K. (2015). A simple and high-resolution stereolithography-based 3D bioprinting system using visible light crosslinkable bioinks. *Biofabrication*, 7(4), 045009.

15. Schaedler, T. A., and Carter, W. B. (2016). Architected cellular materials. *Annual Review of Materials Research*, 46, 187-210.

16. Ge, Q., Li, Z., Wang, Z., Zhang, W., He, X., Zhou, J., and Fang, N. (2020). Projection Micro Stereolithography Based 3D Printing and Its Applications. *International Journal of Extreme Manufacturing*. https://iopscience.iop.org/article/10.1088/2631-7990/ab8d9a

17. Ovsianikov, A. and Chichkov, B.N. (2012). Three-dimensional microfabrication by two-photon polymerization technique. *Methods Mol. Biol*. 868, 311–325.

18. Ge, Q., Sakhaei, A. H., Lee, H., Dunn, C. K., Fang, N. X., and Dunn, M. L. (2016). Multimaterial 4D Printing with Tailorable Shape Memory Polymers. *Scientific Reports*, 6, 31110.

19. Sun, C., Fang, N., Wu, D. M., and Zhang, X. (2005). Projection micro-stereolithography using digital micro-mirror dynamic mask. *Sensors and Actuators A: Physical*, 121(1), 113-120.

20. Gauvin, R., Chen, Y. C., Lee, J. W., Soman, P., Zorlutuna, P., Nichol, J. W., Bae, H. Chen, S. and Khademhosseini, A. (2012). Microfabrication of complex porous tissue engineering scaffolds using 3D projection stereolithography. *Biomaterials*, 33(15), 3824-3834.

21. Tumbleston, J. R., Shirvanyants, D., Ermoshkin, N., Janusziewicz, R., Johnson, A. R., Kelly, D., et al. (2015). Continuous liquid interface production of 3D objects. *Science*, 347(6228), 1349-1352.

22. Jacobsen, A. J., Barvosa-Carter, W., and Nutt, S. (2007). Micro-scale truss structures formed from self-propagating photopolymer waveguides. *Advanced Materials*, 19(22), 3892-3896.

23. Moroni, L., De Wijn, J. R., and Van Blitterswijk, C. A. (2006). 3D fiber-deposited scaffolds for tissue engineering: influence of pores geometry and architecture on dynamic mechanical properties. *Biomaterials*, 27(7), 974-985.

24. Giordano, R. A., Wu, B. M., Borland, S. W., Cima, L. G., Sachs, E. M., and Cima, M. J. (1997). Mechanical properties of dense polylactic acid structures fabricated by three dimensional printing. *Journal of Biomaterials Science, Polymer Edition*, 8(1), 63-75.

25. Pfister, A., Landers, R., Laib, A., Hübner, U., Schmelzeisen, R., & Mülhaupt, R. (2004). Biofunctional rapid prototyping for tissue-engineering applications: 3D bioplotting versus 3D printing. *Journal of Polymer Science Part A: Polymer Chemistry*, 42(3), 624-638.

26. Deitzel, J. M., Kleinmeyer, J., Harris, D. E. A., and Tan, N. B. (2001). The effect of processing variables on the morphology of electrospun nanofibers and textiles. *Polymer*, 42(1), 261-272.

27. Bashur, C.A. et al. (2006) Effect of fiber diameter and orientation on fibroblast morphology and proliferation on electrospun poly(D,L-lactic-co-glycolic acid) meshes. *Biomaterials,* 27, 5681–5688

28. Shusteff, M., Browar, A. E. M., Kelly, B. E., Henriksson, J., Weisgraber, T. H., Panas, R. M. (2017). One-step volumetric additive manufacturing of complex polymer structures. *Science Advances*, 3(12), eaao5496.

29. Kelly, B. E., Bhattacharya, I., Heidari, H., Shusteff, M., Spadaccini, C. M., and Taylor, H. K. (2019). Volumetric additive manufacturing via tomographic reconstruction. *Science*, 363(6431), 1075-1079.

30. Beer, M. P., Laan, H. L., Cole, M. A., Whelan, R. J., Burns, M. A., and Scott, T. F. (2019). Rapid, continuous additive manufacturing by volumetric polymerization inhibition patterning. *Science advances*, 5(1), eaau8723.

31. Leung, Y. S., Kwok, T. H., Li, X., Yang, Y., Wang, C. C., & Chen, Y. (2019). Challenges and status on design and computation for emerging additive manufacturing technologies. *Journal of Computing and Information Science in Engineering*, 19(2).

32. Guzzi, E. A., and Tibbitt, M. W. (2020). Additive manufacturing of precision biomaterials. *Advanced Materials*, 32(13), 1901994.

33. Chen, X., Liu, W., Dong, B., Lee, J., Ware H.O.T., Zhang, H. F., et al. (2018). High-Speed 3D Printing of Millimeter-Size Customized Aspheric Imaging Lenses with Sub 7 nm Surface Roughness. *Advanced Materials*, 30(18), 1705683.

34. Urrios, A., Parra-Cavrera, C., Bhattacharjee, N., Gonzalez-Suarez, A. M., Rigat-Brugarolas, L. G., Nallapatti, U., et al. (2016). 3D-printing of transparent bio-microfluidic devices in PEG-DA. *Lab on a Chip*, 16(12), 2287-2294.

35. Cutmann, B., Kockinger, M., Glotz, G., Ciaglia, T., Slama, E., Zadravec, M., et al. (2017). Design and 3D printing of a stainless steel reactor for continuous difluoromethylations using fluoroform. *Reaction Chemistry & Engineering*, 2(6), 919-927.

36. Osanov, M., and Guset, J. K. (2016). Topology Optimization for Architected Materials Design. *Annual Review of Materials Research*, 46, 211-233.

37. Okkels, F., and Bruus, H. (2007). Scaling behavior of optimally structured catalytic microfluidic reactors. *Physical Review E*, 75(1), 016301.

38. Bai, H., Theuerkauf, J., Gillis, P. A., and Witt, Paul. M. (2009). A Coupled DEM and CFD Simulation of Flow Field and Pressure Drop in Fixed Bed Reactor with Randomly Packed Catalyst Particles. *Industrial & Engineering Chemistry Research*, 48(8), 4060-4074.

39. Torre, A. D., Montenegro, G., Onroati, A., and Tabor, G. (2015). CFD Characterization of Pressure Drop and Heat Transfer Inside Porous Substrates. *Energy procedia*, 81, 836-845.

40. Kao, P.-H., Ren, T.-F., and Yang, R.-J. (2007). An investigation into fixed-bed microreactors using lattice Boltzmann method simulations. *International Journal of Heat and Mass Transfer*, 50(21-22), 4243-4255.

41. Ortega-Casanova, J. (2017). Application of CFD on the optimization by response surface methodology of a micromixing unit and its use as a chemical microreactor. *Chemical Engineering and Processing: Process Intensification*, 117, 18-26.

42. https://www.altair.com/optistruct/

43. http://www.withinlab.com/

44. Tonomura, O., Tanaka, S., and Noda, M. (2004). CFD-based optimal design of manifold in plate-fin microdevices. *Chemical Engineering Journal*, 101(1-3), 397-402.

45. Schapper, D., Fernandes, R. L., Lantz, A. E., Okkels, F., Bruus, H., and Gernaeym, K. V. (2010). Topology optimized microbioreactors. *Biotechnology and Bioengineering*, 108(4), 786-796.

46. Egan PF, Gonella VC, Engensperger M, Ferguson SJ, Shea K (2017). Computationally designed lattices with tuned properties for tissue engineering using 3D printing. *PLOS ONE,* 12(8): e0182902.

47. Kitson, P. J., Marshall, R. J., Long, D., Forgan, R. S., and Cronin, L. (2014). 3D Printed High-Throughput Hydrothermal Reactionware for Discovery, Optimization, and Scale-Up. *Angewandte Chemie International Edition in English*, 53(47), 12723-12728.

4825. Capel, A. J., Edmondson, S., Christie, S. D. R., Goodridge, R. D., Bibb, R. J., and Thurstans, M. (2013). Design and additive manufacture for flow chemistry. *Lab on a Chip*, 13(23), 4583-4590.

49. Rossi, S., Porta, R., Brenna, D., Puglisi, A., and Benaglia, M . (2017). Stereoselective Catalytic Synthesis of Active Pharmaceutical Ingredients in Homemade 3D-Printed Mesoreactors. *Angewandte Chemie*, 56(15), 4290-4294.

50. Sochol, R.D., Sweet, E., Glick, C.C., Venkatesh, S., Avetisyan, A., Ekman, K.F., et al. (2016). 3D printed microfluidic circuitry via multijet-based additive manufacturing. *Lab on a Chip*, 16(4), 668-678.

51. Gong, H., Woolley, A. T., and Nordin, G. P. (2016). High density 3D printed microfluidic valves, pumps, and multiplexers. *Lab on a Chip*, 16(13), 2450-2458.

52. Bhargava, K. C., Thompson, B., and Malmstadt, N. (2014). Discrete elements for 3D microfluidics. *Proceedings of the National Academy of Sciences*, 111(42), 15013-15018.

53. Symes, M. D., Kitson, P. J., Yan, J., Richmond, C. J., Cooper, G. J. T., Bowman, R. W., et al. (2012). Integrated 3D-printed reactionware for chemical synthesis and analysis. *Nature chemistry*, 4(5), 349-354.

54. Xia, C., and Fang, N. X. 3D microfabricated bioreactor with capillaries. *Biomedical Microdevices*, 11(6), 1309-1315.

55. Roper, C. S., Schubert, R. C., Maloney, K. J., Page, D., Ro, C. J., Yang, S. S., et al. (2015) Scalable 3D Bicontinuous Fluid Networks: Polymer Heat Exchangers Toward Artificial Organs. *Advanced Materials*, 27(15), 2479-2484.

56. Espinosa-Hoyos, D., Jagielska, A., Homan, K. A., Du, H., Busbee, T., Anderson, D. G., et al. (2018). Engineered 3D-printed artificial axons. *Scientific Reports*, 8(1), 478.

57. Ma, X., Qu, X., Zhu, W., Li, Y., Yuan, S., Zhang, H., et al. (2016). Deterministically patterned biomimetic human iPSC-derived hepatic model via rapid 3D bioprinting. *Proceedings of the National Academy of Sciences of the United States of America*, 113(8), 2206-2211.

58. Zhao, Y., Yao, R., Ouyang, L., Ding, H., Zhnag, T., Zhang, K., et al. (2014). Three-dimensional printing of Hela cells for cervical tumor model in vitro. *Biofabrication*, 6(3), 035001.

59. Yang, D., Niu, X., Liu, Y., Wang, T., Gu, X., Song, L., et al. (2018). Electrospun Nanofibrous Membranes: A Novel Solid Substrate for Microfluidic Immunoassays for HIV. *Advanced Materials*, 20(24), 4770-4775.

60. Lee, H., and Cho, D. (2016). One-step fabrication of an organ-on-a-chip with spatial heterogeneity using a 3D bioprinting technology. *Lab on a Chip*, 16(14), 2618-2625.

61. Li, H., Tan, C., and Li, L. (2018). Review of 3D printable hydrogels and constructs. *Materials & Design*, 159, 20-38.

62. Leon, C. P., Hussey, W., Frazao, F., Jones, D., Ruggeri, E., Tzortzatos, S., et al. (2014). The 3D printing of a polymeric electrochemical cell body and its characterisation. *Chemical Engineering Transactions*, 41, 1-6.

63. Guo, N., Leu, M. C., and Koylu, U. O. (2014). Bio-inspired flow field designs for polymer electrolyte membrane fuel cells. *International Journal of Hydrogen Energy*, 39(36), 21185-21195.

64. Chisholm, G., Kitson, P. J., Kirkaldy, N. D., Bloor, L. G., and Cronin, L. (2018). 3D printed flow plates for the electrolysis of water: an economic and adaptable approach to device manufacture. *Energy & Environmental Science*, 7(9), 3026-3032.

65. Hashemi, S. M. H., Karnakov, P., Hadikhani, P., Chinello, E., Litvinov, S., Moser, C., et al. (2019). A versatile and membrane-less electrochemical reactor for the electrolysis of water and brine. *Energy & Environmental Science*, 12(5), 1592-1604.

66. Lee, C., Taylor, A. C., Beirne, S., and Wallace, G. G. (2017). 3D-Printed Conical Arrays of TiO2 Electrodes for Enhanced Photoelectrochemical Water Splitting. *Advanced Energy materials*, 7(21), 1701060.

67. Zhu, C., Qi, Z., Beck, V. A., Luneau, m., Lattimer, J., Chen, W., et al. (2018). Toward digitally controlled catalyst architectures: Hierarchical nanoporous gold via 3D printing. *Science Advances*, 4(8), eaas9459.

68. Tian, X., Jin, J., Yuan, S., Chua, C. K., Tor, S. B., & Zhou, K. (2017). Emerging 3D-printed electrochemical energy storage devices: a critical review. *Advanced Energy Materials*, 7(17), 1700127.

69. Yuan, S., Shen, F., Chua, C. K., & Zhou, K. (2019). Polymeric composites for powder-based additive manufacturing: Materials and applications. *Progress in Polymer Science*, 91, 141-168.

70. Li, R., Yuan, S., Zhang, W., Zheng, H., Zhu, W., Li, B., et al. (2019). 3D Printing of Mixed Matrix Films Based on Metal–Organic Frameworks and Thermoplastic Polyamide 12 by Selective Laser Sintering for Water Applications. *ACS Applied Materials & Interfaces*, 11(43), 40564-40574.

71. Kotz, F., Risch, P., Helmer, D., and Rapp, B. E. (2019). High-Performance Materials for 3D Printing in Chemical Synthesis Applications. *Advanced Materials*, 31(26), 1805982.

72. http://www.car-engineer.com/cordierite-for-catalytic-converters/

73. U.S. EPA Tier 3, https://www.epa.gov/regulations-emissions-vehicles-and-engines/final-rule-control-air-pollution-motor-vehicles-tier-3.

74. Tubio, C. R., Azuaje, J., Escalante, L., Coelho, A., Guitian, F., Sotelo, E., et al. (2016). 3D printing of a heterogeneous copper-based catalyst. *Journal of catalysis*, 334, 110-115.

75. Konarova, M., Aslam, W., Ge, L., Ma, Q., Tang, F., Rudolph, V., et al. (2017). Enabling Process Intensification by 3 D Printing of Catalytic Structures. *ChemCatChem*, 9(21), 4132-4138.

76. Al-Ketan, O., Pelanconi, M., Ortona, A., and Al-Rub, R. K. A. (2019). Additive manufacturing of architected catalytic ceramic substrates based on triply periodic minimal surfaces. *Journal of the American Ceramic Society*, 102(10), 6176-6193.

77. Zhou, X., and Liu, C. (2017). Three-dimensional Printing for Catalytic Applications: Current Status and Perspectives. *Advanced Functional Materials*, 27(30), 1701134.

78. Hensleigh, R. M., Cui, H., Oakdale, J. S., Ye, J. C., Campbell, P. G., Duoss, E. B., et al. (2018). Additive manufacturing of complex micro-architected graphene aerogels. *Materials Horizons*, 5(6), 1035-1041.

79. Zhu, C., Han, Y., Duoss, E. B., Golobic, A. M., Kuntz, J. D., Spadaccini, C. M., et al. (2015). Highly compressible 3D periodic graphene aerogel microlattices. *Nature Communications*, 6(1), 6962.

80. Zhakeyev, A., Wang, P., and Zhang, L. (2017). Additive Manufacturing Unlocking the Evolution of Energy Materials. *Advanced Science*, 4(10), 1700187.

81. Sun, K., Wei, T., Ahn, B. Y., Seo, J. Y., Dillon, S. J., and Lewis, J. A. (2013). 3D Printing of Interdigitated Li-Ion Microbattery Architectures. *Advanced Materials*, 25(33), 4539-4543.

82. Saleh, M. S., Li, J., Park, J., and Panat, R. (2018). 3D printed hierarchically-porous microlattice electrode materials for exceptionally high specific capacity and areal capacity lithium ion batteries. *Additive Manufacturing*, 23, 70-78.

83. Xu, C., Gallant, B. M., Wunderlich, P. U., Lohmann, T., and Greer, J. R. (2015). Three-Dimensional Au Microlattices as Positive Electrodes for Li–O2 Batteries. *ACS nano*, 9(6), 5876-5883.

84. Cambie, D., Zhao, F., Hessel, V., Debije, M. G., and Noel, T. (2016). A Leaf-Inspired Luminescent Solar Concentrator for Energy-Efficient Continuous-Flow Photochemistry. *Angewandte Chemie international Edition*, 56(4), 1050-1054.

85. Zhao, F., Cambie, D., Janse, J., Wieland, E. W., Kuijpers, K. P. L., Hessel, V., et al. (2018). Scale-up of a Luminescent Solar Concentrator-Based Photomicroreactor via Numbering-up. *ACS Sustainable Chemistry & Engineering*, 6(1), 422-429.

86. Leung, Y.-S., Kwok, T.-H., Li, X., Yang, Y., Wang, C. C. L., and Chen, Y. (2019). Challenges and Status on Design and Computation for Emerging Additive Manufacturing Technologies. *Journal of Computing and Information Science in Engineering*, 19(2), 021013.

87. Vaezi, M., Chianrabutra, S., Mellor, B., and Yang, S. Multiple material additive manufacturing – Part 1: a review, *Virtual and Physical Prototyping*, 8(1), 19-50.

88. Lind, J. U., Busbee, T. A., Valentine, A. D., Pasqualini, F. S., Yuan, H., Yadid, M., et al. (2016). Instrumented cardiac microphysiological devices via multimaterial three-dimensional printing. *Nature Materials*, 16, 303-308.

89. Mayer, F., Richter, S., Westhauser, J., Blasxo, E., Barner-Kowollik, C., and Wegener, M. (2019). Multimaterial 3D laser microprinting using an integrated microfluidic system. *Science Advances*, 5(2), eaau9160.

90. MacDonald, E., and Wicker, R. (2016). Multiprocess 3D printing for increasing component functionality. *Science*, 353(6307), aaf2093.

91. Chu, W.-S., Kim, M.-S., Jang, K.-H., Song, J.-H., Rodrigue, H., Chun, D.-M., et al. (2016). From design for manufacturing (DFM) to manufacturing for design (MFD) via hybrid manufacturing and smart factory: A review and perspective of paradigm shift. *International Journal of Precision Engineering and Manufacturing-Green Technology*, 3(2), 209-222.

92. Yoon, H.-S., Jang, K.-H., Kim, E., Lee, H.-T., and Ahn, S.-H. (2017). Hybrid 3D printing by bridging micro/nano processes. *International Journal of Precision Engineering and Manufacturing-Green Technology*, 27(6), 065006.

93. Yoon, H.-S., Lee, H.-T., Jang, K.-H., Kim, C.-S., Park, H., Kim, D.-W., et al. (2017). CAD/CAM for scalable nanomanufacturing: A network-based system for hybrid 3D printing. *Microsystems & Nanoengineering*, 3, 17072.

94. Lim, J., Kim, Y. K., Won, D. J., Choi, I. H., Lee, S., and Kim, J. (2019). 3D Printing of Freestanding Overhanging Structures Utilizing an In Situ Light Guide. *Advanced Materials Technologies*, 4(8), 1900118.

95. Kim, D.-H., Kim, T. J. Y., Wang, X., Kim, M., Quan, Y.-J., Oh, J. W., et al. (2018). Smart Machining Process Using Machine Learning: A Review and Perspective on Machining Industry, *International Journal of Precision Engineering and Manufacturing-Green Technology*, 5(4), 555-568.

96. Qi, X., Chen, G., Li, Y., Cheng, X., and Li, C. (2019). Applying Neural-Network-Based Machine Learning to Additive Manufacturing: Current Applications, Challenges, and Future Perspectives, *Engineering*, 5(4), 721-729.

97. Zhou, Z., Li, X., and Zare, R. N. (2017). Optimizing Chemical Reactions with Deep Reinforcement Learning. *ACS central Science*, 3(12), 1337-1344.

98. Edington, C. D., Chen, W. L. K., Geishecker, E., Kassis, T., Soenksen, L. R., hushan, B. M., et al. (2018). Interconnected Microphysiological Systems for Quantitative Biology and Pharmacology Studies. *Scientific Reports*, 8, 4530.

99. Malinauskas, M., Zukauskas, A., Hasegawa, S., Hayasaki, Y., Mizeikis, V., Buividas, R., et al. (2016). Ultrafast laser processing of materials: from science to industry. *Light: Science & Applications*, 5(8), e16133.

100. Hansen, C. J., Saksena, R., Kolesky, D. B., Vericella, J. J., Kranz, S. J., Muldowney, G. P., et al. (2012). High-throughput printing via microvascular multinozzle arrays, *Advanced Materials*, 25(1), 96-102.

101. Xu, B., Du, W.-Q., Li, J.-W., Hu, Y.-L., Yang, L., Zhang, C.-C., et al. (2016). High efficiency integration of three-dimensional functional microdevices inside a microfluidic chip by using femtosecond laser multifoci parallel microfabrication, *Scientific Reports*, 6, 19989.

102. Chang, J., Lee, S., Lee, K. B., Lee, S., Cho, Y. T., Seo, J., et al. (2015). Overlay accuracy on a flexible web with a roll printing process based on a roll-to-roll system. *The Review of scientific instruments*, 86(5), 055108.

103. Hempel, M., Lu, A.-Y., Hui. F., Kpulun, T., Lanza, M., Harris, G., et al. (2018). Repeated roll-to-roll transfer of two-dimensional materials by electrochemical delamination. *Nanoscale*, 10(2), 5522-5531.

104. Liang, H.-L., Bay, M. M., Vadrucci, R., Barty-King, C. H., Peng, J., Baumberg, J. J., et al. (2018). Roll-to-roll fabrication of touch-responsive cellulose photonic laminates. *Nature Communication*, 9(1), 4632.

105. Hiltunen. J., Liedert, C., Hiltunen, M., Huttunen, O.H., Hiitola-Keinanen, J., Aikio, S., et al. (2018). Roll-to-roll fabrication of integrated PDMS-paper microfluidics for nucleic acid amplification. *Lab on a Chip*, 18(11), 1552-1559.

106. Wang, Q., Jackson, J. A., GE, Q., Hopkins, J. B., Spadaccini, C. M., and Fang, N. X. (2016). Lightweight Mechanical Metamaterials with Tunable Negative Thermal Expansion. *Physical Review Letter*, 117, 175901.